



ELSEVIER

J. Non-Newtonian Fluid Mech., 54 (1994) 45–86

Journal of
Non-Newtonian
Fluid
Mechanics

Aggregation and dispersion of spheres falling in viscoelastic liquids [☆]

D.D. Joseph, Y.J. Liu, M. Poletto, J. Feng

Department of Aerospace Engineering and Mechanics, University of Minnesota, 107 Akerman Hall, 110 Union Street, Minneapolis, MN 55455, USA

Received 8 November 1993

Abstract

This paper focuses on the settling on one sphere near another or near a wall. We find maximum differences between Newtonian and viscoelastic liquids, with repulsion between nearby bodies in the Newtonian case and attraction in the viscoelastic case. Side-by-side arrangements of sedimenting spheres are unstable in exactly the same way that broadside-on settling of long bodies is unstable at subcritical speeds in a viscoelastic fluid. The line of centers between the spheres rotates from across to along the stream as the spheres are sucked together. The resulting chain of two spheres is a long body which is stable when the line between centers is parallel to the fall, but this configuration breaks up at subcritical speeds where inertia again dominates. To explain the orientation of particles in the supercritical case, we correlate the aggregative power of a viscoelastic fluid with a zero shear value of the coefficient of ratio of the first normal stress difference to the shear stress and for exceptional cases we introduce the idea of the memory of shear-thinning leading to corridors of reduced viscosity.

Keywords: Aggregation of spheres; Dispersion of spheres; Elastic stress ratio; Newtonian liquids; Numerical simulation; Settling of spheres; Sphere–sphere interaction; Viscoelastic liquids; Wall–sphere interaction

1. Introduction

Liu and Joseph [1] discussed the sedimentation of cylinders and flat plates in viscoelastic and Newtonian liquids, noting that the flow-induced anisotropy of

[☆] Dedicated to Professor K. Walters FRS on the occasion of his 60th birthday.

sedimenting spherical particles is associated with the natural orientation of long bodies, longside parallel to the stream when viscoelasticity dominates and perpendicular to the stream when inertia dominates. They reviewed the literature in the sedimentation of long bodies. Joseph and Liu [2] did further experiments on the orientation of a cylinder settling in viscoelastic and pseudoplastic fluid and attempted to identify the main mechanisms controlling orientation. They stressed the fluid's ability to remember where it was thinned and introduced the notion of evanescent corridors of reduced viscosity. In this paper we highlight the importance of the elastic stress ratio N_1/τ , which turns out to be a subtle measure of fluid elasticity.

This paper focuses on the settling of one sphere near another or near a wall. Again we find maximum differences between Newtonian and viscoelastic liquids, with repulsion between nearby bodies in the Newtonian case and attraction in the viscoelastic case. This observation has applications for manipulative strategies addressing the problem of placements of particles by flowing liquids.

Christopherson and Dowson [3] took notice of a tendency for balls to rotate and fall off-center while settling in Newtonian liquids in a cylindrical container. Tanner [4] noticed that this tendency is enhanced in non-Newtonian liquids, stating that "if one carefully drops the balls axially in the fall tube, there appears to be a critical ball/tube radius after which the ball is seen to fall off-center and rotate." The critical radius ratio may possibly be associated either with a critical fall speed or with other critical values associated with instability. The effects of eccentricity on the precision of falling ball viscometry were discussed by Caswell [5].

Many papers treat problems of sedimentation of spheres in Stokes flow (Leal [6,7] are convenient references). Goldman, et al. [8] treat the problem of interaction between a sphere and a wall. They also consider the problem of a sphere "rolling" down an inclined wall and find that the sphere cannot be in physical contact with the wall and that it slips, giving rise to anomalous rotation when forced into close approach. Bungay and Brenner [9] showed that the rotation of a tightly fitting ball falling down a vertical tube would change sign as the distance between the ball and the tube wall tends to zero. These Stokes flow predictions involve neither inertia nor elasticity. The phenomenon of anomalous rolling predicted by these authors appears in the experiments of Humphrey and Murata [10] who found that the rotation of a sphere gradually changes from positive (opposite to downhill rolling) to negative (in the sense of downhill rolling) as the tube inclination angle is increased and the sphere contacts the wall. They conclude that inertia induced lift keeps the rolling ball off the wall at the smaller angles of inclination.

Joseph, et al. [11] found anomalous rolling of a sphere in viscoelastic liquids along an inclined path. The angle between the wall and the direction of gravity is varied from zero to 45° . A sphere falling down these inclined walls rotates as if falling down the wall in viscous liquids as it does in dry rolling, but rotates as if rolling up the wall against intuition in viscoelastic liquid. Liu et al. [12] documented this phenomenon with measured data.

Sigli and Coutanceau [13,14] studies the effects of the walls of a round tube on a sphere settling under gravity. Like Tanner [4], they noted that there are critical

ball/tube radii for off-center positions. A small initial eccentricity is magnified by the effects of the fluid's elasticity. It is likely that the sense of rotation of a sphere falling off-center in a tube filled with viscoelastic liquid is anomalous.

Riddle et al. [15] presented an experimental investigation in which the distance between two identical spheres falling along their line of centers in a viscoelastic fluid was determined as a function of time. They found that, for all five fluids used in the experiments, the spheres attract if they are initially close and separate if they are not close. There is a critical separation distance. We shall show that there is also a critical separation for side-by-side attraction. This suggests that the critical separation distance for end-to-end settling may not be associated with a negative wake as has been suggested by Bird et al. [16].

Lateral migration and chaining of spheres in a 0.5% aqueous polyacrylamide solution and in a solution of high molecular weight polyisobutylene in a low molecular weight polyisobutylene were observed by Michele et al. [17] in experiments using very tiny spheres (60–70 μm). A droplet of the suspension was placed between two glass plates that were pushed together as close as possible (about 100 μm). Different kinds of aggregation were observed in rectilinear and rotary shear. They also showed chaining and lateral migration of these tiny spheres in an elongational flow by pulling a glass plate out of a droplet of the suspension. The aggregation of particles appears to be a generic feature of flows of viscoelastic fluids that occurs in many different types of fluids, for vastly different scales and types of motion.

Brunn [18] did a theoretical analysis of the interaction between spheres in a second order fluid with inertia neglected and although he found an attractive force drawing the spheres together he did not find a critical separation distance for attraction. Brunn's analysis cannot treat close approach because it has been assumed that the distance between sphere centers is large. His results, as far as they go, are consistent with our observations and suggest that the mechanism involved is associated with the normal stresses, which are in his analysis, and not with shear-thinning, which is neglected in his analysis. In fact, shear-thinning plus memory may play an important role, at least in the chaining of spheres, as we shall see.

Giesekus [19] tried to explain end-to-end and side-to-side attractions in terms of normal stresses using second order theory with inertia neglected, like Brunn. These two authors could not explain the critical separation distance observed by Riddle et al. [15] and they did not investigate the possibility that this distance is determined by a competition of non-Newtonian and inertial effects.

As far as we know, ours is the first study of side-by-side sphere–sphere attraction. We find that the spheres attract when the initial separation distance is smaller than a critical value and they do not attract when the initial distance is larger than this critical distance. The side-by-side spheres never attract in a Newtonian fluid; if they are initially separated by a small distance, they repel each other; just the opposite of their behavior in a viscoelastic fluid.

Side-by-side arrangements of sedimenting spheres are unstable in exactly the same way that broadside-on settling of long bodies is unstable at subcritical speeds

in a viscoelastic fluid [1,2]. The line of centers between the spheres rotates from across to along the stream as the spheres are sucked together. The resulting chain of two spheres is a long body that is stable when the line between centers is parallel to the fall, but this configuration breaks up at supercritical speeds in which inertia again dominates. These authors have presented evidence that the critical fall velocity is not too much greater than the measured value of the shear wave speed in nearly all cases.

Van der Brule and Gheissary [20] saw a videotape (shown at the International Congress of Rheology) of the experiments of Joseph and Liu on sedimenting spheres, which form long chains in all viscoelastic liquids at the slow fall speeds in which long bodies rotate with their long side parallel to the fall. This stimulated them to undertake experiments of their own on sedimenting spheres. They attempted to isolate the effects of shear-thinning and normal stresses by using test fluids that have one and not the other of these properties. They dropped spheres in aqueous polyacrylamide, an ordinary viscoelastic fluid with large normal stresses and strong shear-thinning, and found results identical to ours. Then they did experiments in “shellflo”, an aqueous Xanthan solution that has no measureable normal stresses in shear but is strongly shear-thinning. They found that the spheres chained in this fluid in much the same way that they did in the aqueous polyacrylamide. This suggests that shear-thinning is the important parameter. They then did experiments in a Boger fluid that they prepared with small amounts of polyacrylamide (100 ppm) in glycerin and water. This is a very viscous fluid with large but saturated normal stresses, which leads to constant values of the recoverable shear at high rates of shear. They did not observe chaining in this Boger fluid, and thus concluded that shear-thinning, not elasticity, is the mechanism controlling the chaining of spheres.

Joseph and Liu [2] did experiments on sedimenting cylinders in liquids like the ones used by Van der Brule and Gheissary [20]. They found that in 0.3% aqueous Xanthan (Kelco) and 0.4% Carbopol in 50/50 glycerin–water solutions (see Figs 11 and 12 in Ref. [2]) which are shear-thinning fluids without normal stresses, the cylinder puts its long side parallel to gravity when falling at speeds less than critical. The critical speed in the Xanthan solution was the shear wave speed measured on our meter, but the critical speed for Carbopol was 1/10 the value measured on the meter, the only exception so far. In other respects the Carbopol solution, we shall see, is nearer to Newtonian than to viscoelastic. Spherical particles dropped in the 0.4% Carbopol did not exhibit side-by-side attraction; they repelled each other when they were initially together as in Newtonian fluids. They were repelled by a vertical wall and exhibited only the feeblest form of anomalous rolling (Liu et al. [12]), and apparently no chaining.

These results are surprising because they appear to associate strange effects like tilting and chaining with shear-thinning rather than with normal stresses. In fact, theoretical results for second order fluids, without shear-thinning, give rise to all the observed effects, so we are confronted with a real mystery.

In the case of fluids without normal stress, which do not climb a rod, we may entertain the idea that second order correlations to viscous behavior are negligible, so that we might learn something important at the next non-trivial third order.

Thinking more globally, Joseph and Liu [2] introduced the idea that a combination of memory with shear-thinning is required and may be enough to induce nose-down turning and the related chaining of spheres. They concluded that shear-thinning alone affects the particle's orientation much less, because, like the Carbopol solution, although it shear-thins, the thinning is not persistent and decays very rapidly. The Xanthan solution remembers the place where the viscosity was reduced, to that the back part of a nose-down cylinder, or the spheres behind the lead sphere in a chain, experience a smaller viscosity than the leading end of the cylinder or leading sphere. We might think that corridors of reduced viscosity are marked on the fluid by shear-thinning as a particle drops in the fluid and persist for a time before they relax.

These theories could be tested with standard test liquids provided that they shear-thin and have long memories, whether or not they exhibit normal stresses or climb rods.

The existence of relaxing corridors of reduced viscosity, marked on the fluid by the shear-thinning induced by a falling ball, is consistent with the observations of Cho and Hartnett [21] and Cho et al. [22]. They studied falling ball rheometry, measuring the drag on balls that were dropped in the test liquid in specified and definite intervals of time. They found the same memory effects that we did, effects that were particularly evident in a 10^4 ppm by wt. solution of aqueous polyacrylamide (Separan, AP-273), a highly viscoelastic and highly shear-thinning liquid. The measured terminal velocity depended strongly on the time interval between the dropping of successive balls in the cylinder. Balls launched after only a short wait period would fall up to nearly twice as fast as the speed of the initial ball, and it took intervals of 30 min or more for the memory of the corridor of reduced viscosity to relax.

We can image the trailing spheres in a chain or the trailing end of a long particle setting itself in a corridor of reduced viscosity. For this behavior to occur, shear-thinning and the memory of shear-thinning are required. We should recall at this point that similar effects in weaker form occur in our constant viscosity fluid (STP) and in stronger form in S1 where the degree of shear-thinning is small. Thus shear-thinning plus memory cannot explain everything. The experiments with semidilute Xanthan are interesting because shear-thinning and memory are present, but many other mechanisms that could come into play are absent.

Joseph and Liu [2] considered the possibility that the memory of shear thinning with negligible normal stresses might be modeled with a White–Metzner model using the empirical viscosity function of the rate of shear and a relaxation function which drops to low values faster than the viscosity as the shear rate increases (see Liao et al. [23]). This model is not satisfactory because a healing mechanism for the slow recovery of viscosity after shearing is not accommodated. Besides relaxation we need a healing time, large when the shear is large, which vanishes when there is no shear. We may design such a model by introducing the healing time as a retardation time $\lambda_2(\dot{\gamma})$ which vanishes when $\dot{\gamma} = 0$ and increases to a plateau value of, say half an hour at some finite rate of shear. The model we propose then is of the form

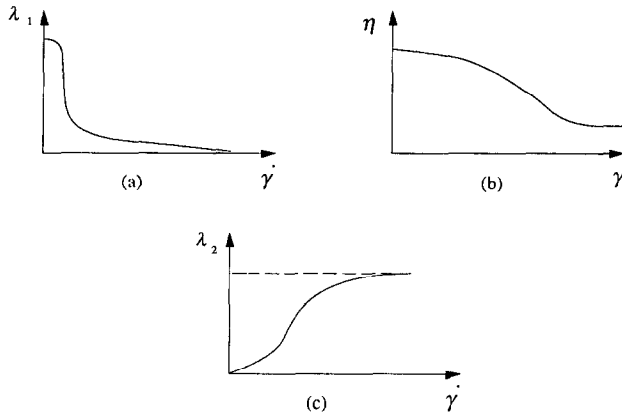


Fig. 1. (a) Relaxation function; (b) viscosity function; (c) retardation function.

$$\lambda_1(\dot{\gamma})\overset{\nabla}{\tau} + \tau = 2\eta(\dot{\gamma})[\mathbf{D} + \lambda_2(\dot{\gamma})\overset{\nabla}{\mathbf{D}}]$$

where $\lambda_1(\dot{\gamma})$, $\eta(\dot{\gamma})$ and $\lambda_2(\dot{\gamma})$ have the aforementioned forms (see Fig. 1), the model will have the desired properties; shear thinning in steady flow, slow relaxation of $\mathbf{D}[\mathbf{u}]$ after shearing and wave propagation into rest with shear speed given by $\sqrt{\eta(0)/\rho\lambda_1(0)}$. This model is presently under investigation.

2. Material and dimensionless parameters

The material parameters that were measured in the liquids used in the experiments are the density ρ , viscosity $\eta = k\dot{\gamma}^{n-1}$, where $\dot{\gamma}$ is the shear rate in reciprocal seconds, the climbing constant $\hat{\beta}$ measured on a rotating rod viscometer (Beavers and Joseph [24]) and the wave speed c . To compute $\hat{\beta}$ from measured values of the climb we need the interfacial tension that we measured with a spinning drop tensiometer (Joseph et al. [25]). The value of $\hat{\beta}$ is insensitive to a small change of surface tension (Chapter 16 in Ref. [26]). Table 1 is the summary of material parameters.

The climbing constant $\hat{\beta}$ is related to the limiting (zero shear) value of the first and second normal stress differences

$$(\psi_{10}, \psi_{20}) = \lim_{\dot{\gamma} \rightarrow 0} [N_1(\dot{\gamma}), N_2(\dot{\gamma})]/\dot{\gamma}^2, \tag{2.1}$$

by

$$\hat{\beta} = \frac{1}{2}\psi_{10} + \psi_{20}. \tag{2.2}$$

The climbing constant

$$\hat{\beta} = 3\alpha_1 + 2\alpha_2, \tag{2.3}$$

may also be expressed in terms of quadratic constants

$$(\alpha_1, \alpha_2) = (-\frac{1}{2}\psi_{10}, \psi_{10} + \psi_{20}), \tag{2.4}$$

of the second order fluid. $\alpha_2/|\alpha_1|$ is the ratio of quadratic constants and

$$[\alpha_1, \alpha_2] = (-m, 2m - 2)\hat{\beta}/(m - 4), \quad (2.5)$$

where $m = 2\alpha_1/(2\alpha_1 + \alpha_2) = -\psi_{10}/\psi_{20}$ is the ratio of the first to second normal stress differences. It can be argued (Section 17.11 in Ref. [26]) that $m = 10$ is a reasonable value for our polymer solutions. Then

$$\frac{\alpha_2}{|\alpha_1|} = \left| \frac{2(1 - m)}{m} \right| = 1.8, \quad (2.6)$$

is a constant and α_1 and α_2 are determined by the measured values of the climbing constant $\hat{\beta}$. We are going to assume (2.6) in the calculations that follow. The value of ψ_{10} that we get from measuring $\hat{\beta}$ is not sensitive to the value of the ratio ψ_{20}/ψ_{10} as long as ψ_{20} is relatively small and negative (see Section 17.11 in Ref. [26]).

The measured value of the climbing constant, together with the assumption that the second normal stress difference is $-1/10$ as large as the first, allows us to evaluate Roscoe's [27] formula

$$T_{11} - T_{22} = 3\dot{s}\eta_0 + 3(\alpha_1 + \alpha_2)\dot{s}^2 \quad (2.7)$$

for the extensional stress difference, where \dot{s} is the rate of stretching in the direction x_1 and η_0 is the zero shear viscosity. Using (2.6) and $\alpha_1 = -\psi_{10}/2$ we get

$$T_{11} - T_{22} = 3\dot{s}\eta_0 + 1.2\psi_{10}\dot{s}^2. \quad (2.8)$$

The zero shear value of the first normal stress difference $\psi_{10} = (2m(m - 4))\hat{\beta} = (10/3)\hat{\beta}$ and the zero shear quadratic correction $4\dot{s}\hat{\beta}$ of Trouton's viscosity, $3\eta_0$,

Table 1
Summary of material parameters

Fluid	ρ (g cm ⁻³)	η_0 (Pa.s)	k	n	$\hat{\beta}$ (g cm ⁻¹)	ψ_{10} (g cm ⁻¹)	c (cm s ⁻¹)	λ_0 (s)	$\frac{\psi_{10}}{\eta_0} = \frac{10\hat{\beta}}{3\eta_0}$ (s)
1.5% aqueous polyox	1	17.3	5.71	0.44	132	440	20.3	0.420	2.54
1.25% aqueous polyox	1	12.7	4.21	0.45	117	389	17.2	0.429	3.07
1.0% aqueous polyox	1	7.65	3.97	0.42	108	360	15.0	0.34	4.70
0.4% Carbopol in 50/50 glycerin-water	1.13	0.76	0.31	0.67	0	0	15.9	0.027	0
0.3% aqueous Xanthan	1	5.21	1.1	0.28	0	0	12.2	0.35	0
S1	0.875	8.06	7.14	0.62	11.8	39.3	72.4	0.018	0.49
STP	0.86	18.0	17.8	0.85	0.97	3.23	286	0.0026	0.02

Liu and Joseph [1] did some experiments with the 1.0% aqueous polyox listed in this Table, but not used in the experiments reported here. The stress ratio ψ_{10}/η_0 is a measure for which the more dilute polyox solutions are relatively more elastic.

increase with $\hat{\beta}$. An argument given by Liu and Joseph [1] shows how extensional stresses broadly speaking can control some of the properties of the aggregation of particles in viscoelastic liquids documented here.

Material parameters of the fluids used in our experiments are listed in Table 1. The percent of the polymers and the percent of the glycerin in water are by weight. Glycerin is a Newtonian liquid. Carbopol is basically a non-elastic but shear-thinning fluid. STP is a weakly viscoelastic liquid with small normal stresses and basically constant viscosity (see Fig. 5 in Ref. [24]). For shear rates below 100 s^{-1} , STP could be called a Boger fluid. The polyacrylamide and polyox solutions are standard viscoelastic liquids.

An important measure of elasticity is the elastic stress ratio

$$\frac{N_1(\dot{\gamma}) \stackrel{\text{def}}{=} \psi_1(\dot{\gamma})\dot{\gamma}}{\tau(\dot{\gamma})} = \frac{\psi_1(\dot{\gamma})}{\eta(\dot{\gamma})}, \quad (2.9)$$

where ψ_1/η is the elastic stress ratio coefficient whose limiting $\dot{\gamma} \rightarrow 0$ value is ψ_{10}/η_0 . (The ratio N_1/τ is twice the recoverable shear; see Barnes et al. [28].) This ratio vanishes for Newtonian fluids and is very small for dilute solutions with Newtonian solvents, like Boger fluids. For small values of $\dot{\gamma}$, (2.9) becomes

$$\lim_{\dot{\gamma} \rightarrow 0} \frac{N_1(\dot{\gamma})}{\tau(\dot{\gamma})} \rightarrow \frac{\psi_{10}}{\eta_0} \dot{\gamma}, \quad (2.10)$$

where

$$\frac{\psi_{10}}{\eta_0} \approx \frac{10\hat{\beta}}{3\eta_0}, \quad (2.11)$$

is a material parameter. Values of $10\hat{\beta}/3\eta_0$ are listed in Table 1. The stress ratio coefficient could have a finite and even large value in mobile liquids with small values of η under circumstances in which N_1 and even $\hat{\beta}$ are too small to measure. In this sense, the stress ratio of mobile liquids is indeterminate. We thought at first that this indeterminism might apply to the 0.3% Xanthan solution but the viscosity of Xanthan at the shear rates in our experiments is too large to support any conclusion other than $\hat{\beta}/\eta = 0$.

The stress ratio is not a monotonic function of concentration. Aggregation of particles occurs more readily in fluids with high stress ratios independent of concentration.

The dimensionless parameters used in this study are the Reynolds number

$$Re_0 = \frac{UD}{\eta_0}, \quad (2.12)$$

where U is the terminal velocity of a sphere of radius D , the Weissenberg number

$$W_0 = \frac{\lambda_0 U}{D}, \quad (2.13)$$

where $\lambda_0 = \eta_0/\rho c^2$ is computed from measured values of η and the wave speed c , the Mach number $M^2 = U^2/c^2 = ReW$ and the elasticity $E = \eta\lambda/\rho D^2$. The flows in the experiments reported here are strongly subcritical with $M \ll 1$.

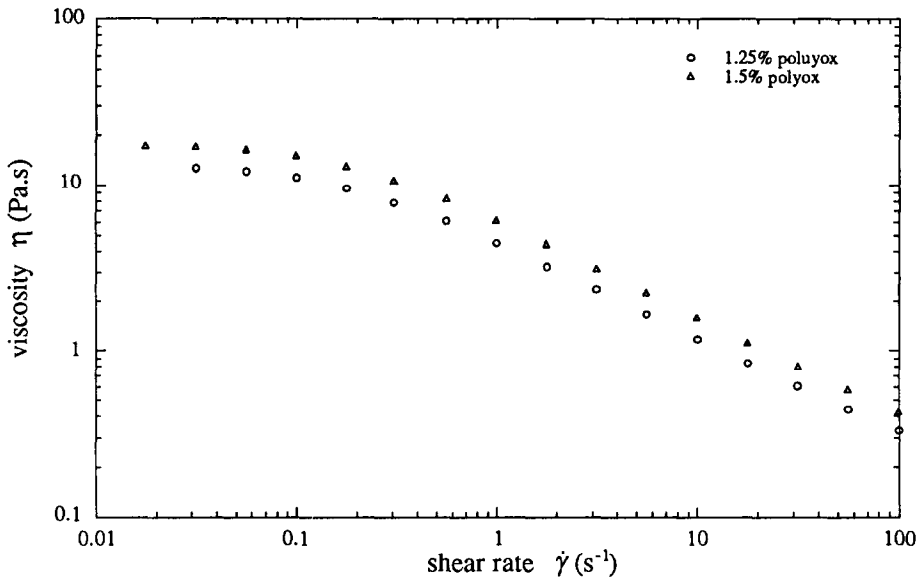


Fig. 2. The viscosities of polyox solutions as a function of the shear rate were measured, at room temperature, on a RSF2 Rheometrics fluid rheometer with a Couette apparatus.

Two different solutions of aqueous polyox (WSR 301) at concentrations of 1.5 and 1.25 wt.% were used as test liquids. Plots of viscosity vs. shear rate for both solutions are given in Fig. 2. Values of dynamic moduli of these two solutions as a function of shear frequency are shown in Fig. 3.

STP is a solution of polyisobutylene (PIB) in petroleum oil that was used extensively in early studies of rod climbing [26]. S1 is a solution of 5 wt.% PIB in decalin plus 50% polybutene oil. The viscosity and the values for the dynamic moduli of these two polymer solutions are shown in Figs. 4 and 5 respectively. The viscosity of STP is nearly constant for shear rates less than 100. The viscosity of S1 decreases with increasing $\dot{\gamma}$, but the decrease is very slow for shear rates less than 10. The viscosity of S1 is an order of magnitude smaller than that of STP; it is a much more mobile liquid. Both solutions climb a rotating rod, but the STP is not a good climber; the climbing constant at a temperature of 26.7°C is 0.97 g cm⁻¹. One can say that STP is a Boger fluid with very weak normal stresses. The climbing constant of S1 at 25°C is 11.8 g cm⁻¹ and S1 can be said to resemble STP with much larger normal stresses especially at low rates of shear. The loss modulus for STP is an order of magnitude higher than for S1. The storage modulus of S1 is larger than for STP for shear rates less than about 10 s⁻¹, and the shear rate at which the loss modulus falls below the storage modulus is much lower in S1 than in STP. It is clear that S1 is a more mobile and much more elastic liquid than STP.

We attempted to isolate the role of shear-thinning by suppressing both normal stresses and elasticity by using a solution of 0.4% Carbopol 690 (Goodrich) in a 50/50 glycerin–water mixture in our attraction experiments. The viscosity vs. shear

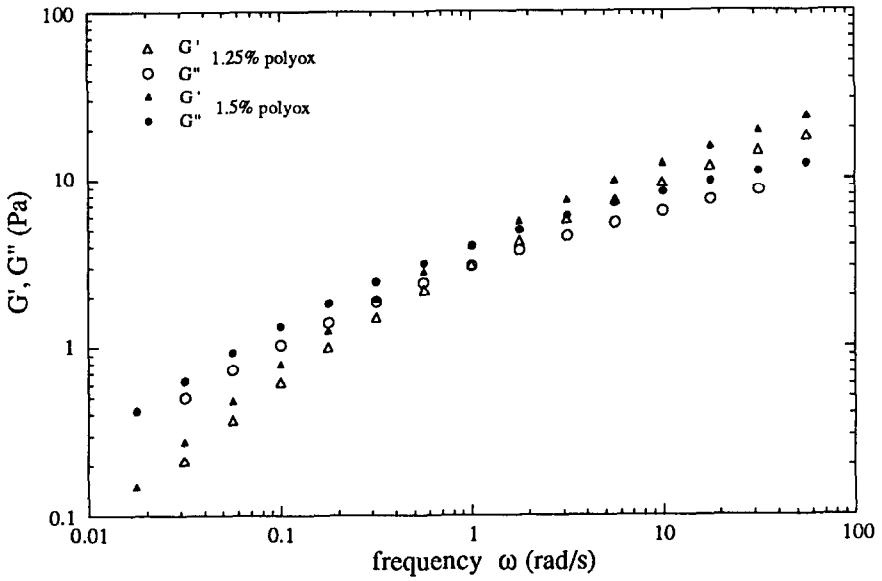


Fig. 3. The dynamic moduli of polyox solutions as a function of the shear frequency were measured, at room temperature, on the same rheometer used for viscosity measurements.

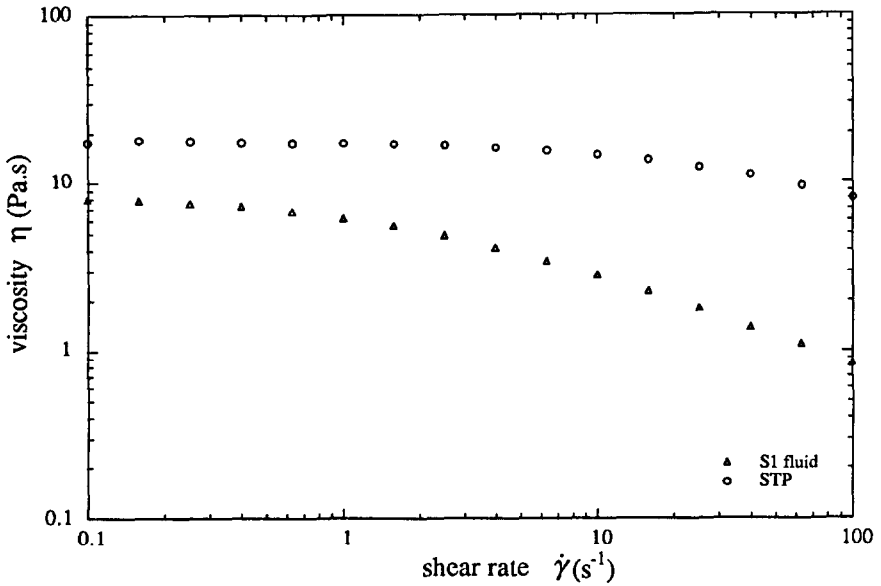


Fig. 4. The viscosities of STP and S1 fluid as a function of the shear rate at temperature of 24.5°C, on a RSF2 Rheometrics fluid rheometer with a cone-plate apparatus. The viscosity of S1 is an order of magnitude smaller than that of STP; it is a much more mobile liquid. S1 is weakly shear-thinning.

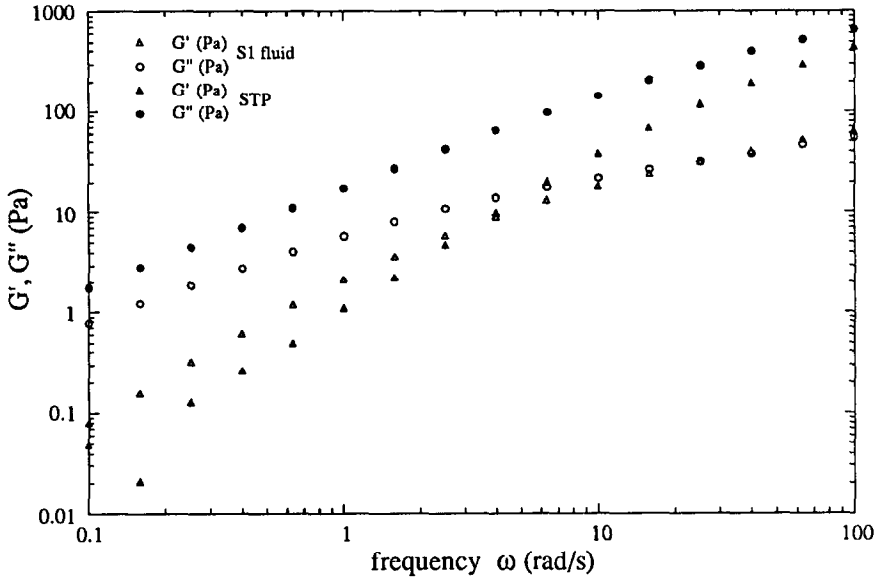


Fig. 5. Dynamic moduli of STP and S1. The loss modulus for STP is an order of magnitude higher than that for S1. The storage modulus of S1 is larger than for STP for shear rates less than about 10. The shear rate at which the loss modulus falls below the storage modulus for S1 is much lower than that for STP.

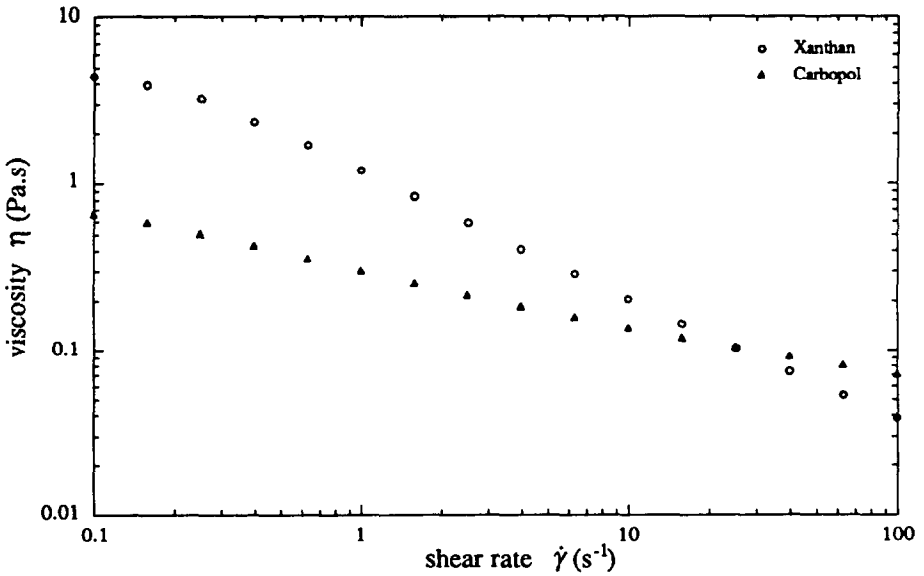


Fig. 6. The viscosities of 0.3% aqueous Xanthan and 0.4% Carbopol in 50/50 glycerin-water solution as a function of the shear rate at temperature of 25.5°C. The Xanthan solution has a higher but more shear-thinning viscosity than the Carbopol solution.

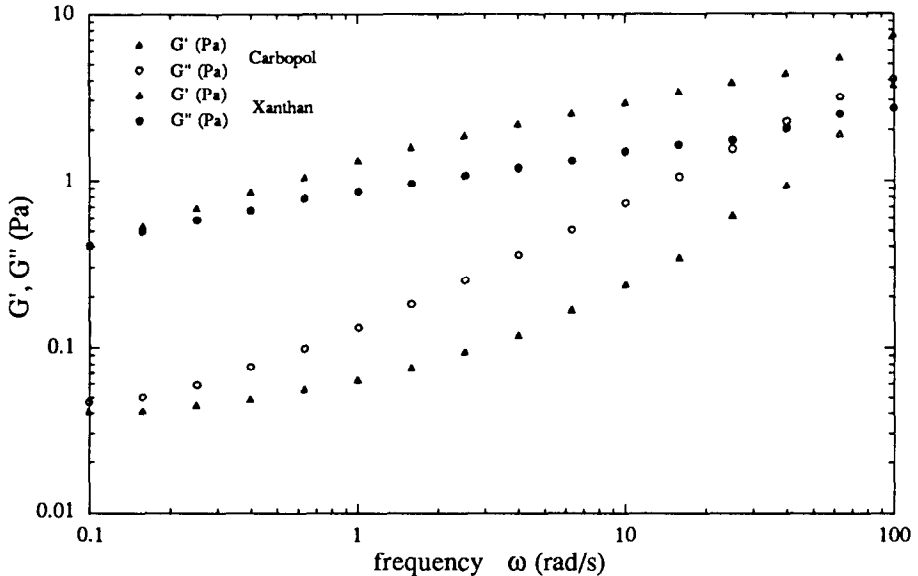


Fig. 7. Dynamic moduli of Xanthan and Carbopol solutions. For modest shear rates ranging from 0.1 to 100, both the storage modulus and loss modulus of the Xanthan solution are higher than those of the Carbopol solution. The storage modulus G' of Xanthan is greater than the loss modulus G'' ; in the Carbopol G'' is greater than G' .

rate for this Carbopol solution is plotted in Fig. 6, and the dynamic moduli are plotted in Fig. 7. Carbopol is thought to be a pseudoplastic fluid without elasticity. Since our Carbopol solution has a non-zero storage modulus, it cannot be said to be without elasticity. The presence of a small elasticity in Carbopol solutions has been noted before. There is no evidence that Carbopol 690 in 50/50 glycerin–water has a measurable value of the first normal stress difference, and it does not climb a rotating rod.

To determine the effects of shear-thinning in a fluid with a strong memory but no normal stresses, we used a solution of 0.3% Xanthan (Kelco) in water. The graph of viscosity vs. shear rate is shown in Fig. 6, and the variation of the storage and loss moduli with frequency is shown in Fig. 7. The Xanthan solution is very shear-thinning and it has no measurable normal stresses. We could not register a first normal stress difference on the Rheometrics fluid rheometer and the 0.3% Xanthan solution would not climb a rotating rod. On the other hand, this fluid has a high storage modulus and can be said to be linearly elastic.

3. Description of the experiments

Spheres were dropped in liquid filled channels made of transparent plexi-glass to allow a video recording of experiments. The first channel, which was used to test

$\frac{1}{4}$ -in spheres, has a gap of 0.44 in, is 6.5 in wide and 25 in high. The second one, which was used to test spheres with different diameters from $\frac{1}{8}$ to $\frac{5}{8}$ in, has a gap of 1 in, is 7 in wide and 30 in high. The motion of sedimenting spheres in these beds is basically two dimensional with spheres centering themselves between two close walls. This centering was described by Liu and Joseph [1]. We did some of our experiments in channels with distant side walls. The phenomena of attraction of nearby bodies in viscoelastic liquids, opposite effects in Newtonian liquids, and anomalous rolling are the same in channels with close and distant side walls. These effects do not depend strongly on the exact distance between the center sphere and the side wall. Velocities and positions of spheres were measured with a video system and image processing software.

To facilitate the side-by-side and simultaneous dropping of two spheres we used a small device which we call the “clothespin dropper”, shown and described in Fig. 8. The same device was also used to release a single sphere at a distance from a straight prismatic rod. The rod was almost as deep as the channel and simulated the presence of a side wall. It was supported by an external support that could be tilted several degrees from the vertical upright position. A sketch of this device is given in Fig. 9. We also used another single sphere dropper to drop spheres with different diameters.

In order to test the effects of sphere diameter, we selected spheres having different diameters and weight, keeping the Reynolds number

$$Re(\dot{\gamma}) = \frac{2aU\rho_1}{\eta} = \text{constant}, \quad (3.1)$$

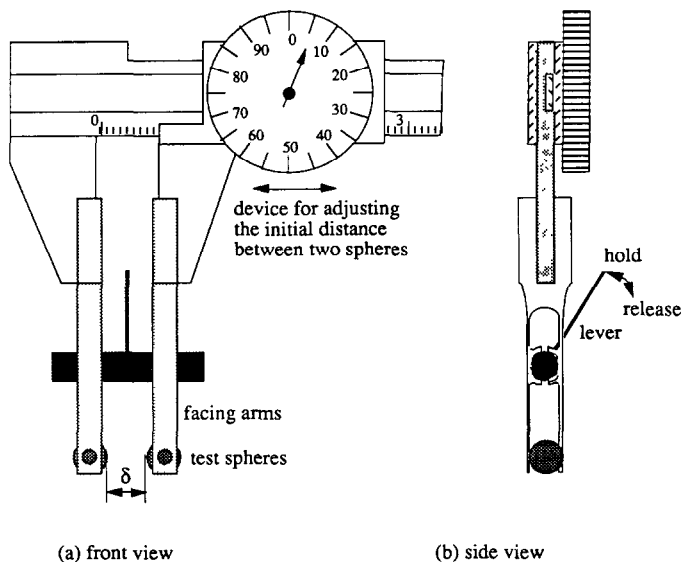


Fig. 8. The “clothespin dropper”. The two spheres are held at the ends of the facing arms. The circular holes on these keep the spheres at the same height. Pulling the level on the facing arms shown in (b) opens the clothespin and releases the two spheres at the same instant.

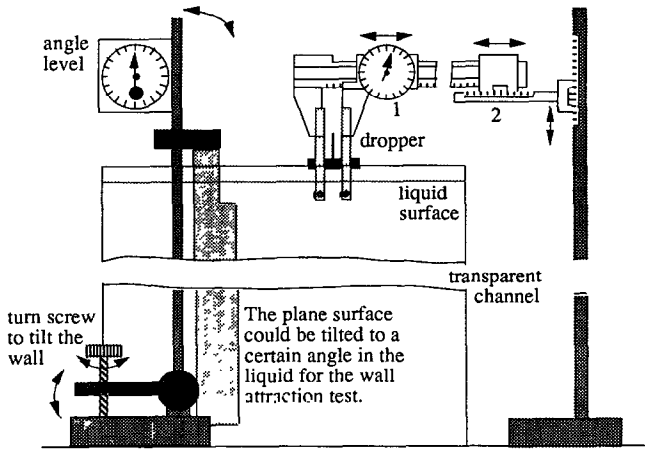


Fig. 9. The front view of the experimental apparatus (not including the video system and image processing system). For the side-by-side test, the initial distance between the two spheres can be adjusted and measured by moving ruler 1; for the wall–sphere test, the initial distance of the sphere from the wall is controlled by ruler 2. The solid plane surface can be inclined by turning the screw and the tilt angle can be measured by the angle level.

where a and U are the radius and the terminal velocity of the sphere, and ρ_s and η are the density and viscosity of liquid, by the following approximate method. Assuming Stokes flow, we have

$$(\rho_s - \rho_l)g\frac{4}{3}\pi a^3 = 6\pi\eta aU, \quad (3.2)$$

where ρ_s is the density of the sphere. The terminal velocity can be determined from Eq. (3.2) as

$$U = \frac{2}{9} \frac{(\rho_s - \rho_l)ga^2}{\eta}. \quad (3.3)$$

The shear rate will be

$$\dot{\gamma} = \frac{U}{2a} = \frac{(\rho_s - \rho_l)ga}{9\eta}. \quad (3.4)$$

Substituting this into the power law equation

$$\eta = \kappa\dot{\gamma}^{n-1}, \quad (3.5)$$

we have

$$\eta = \kappa^{1/n} \left[\frac{(\rho_s - \rho_l)ga}{9} \right]^{(n-1)/n}. \quad (3.6)$$

From Eqs. (3.1) and (3.6), the following condition for determining the diameter and material of spheres can be obtained:

$$(\rho_s - \rho_l)^{2-n}a^{2+n} = \text{constant}. \quad (3.7)$$

Table 2
Spheres tested

Material	Diameter (in.)	Weight (g)	Density (g cm ⁻³)
Tungsten carbide	1/8	0.26	15.8
Steel	1/4	1.02	7.61
Ceramic	7/16	2.74	3.81
Aluminum	5/8	5.78	2.76
Teflon	1/4	0.29	2.18
Aluminum	1/4	0.37	2.76
Tungsten carbide	1/4	2.12	15.8

We chose 1.5% aqueous polyox as the test liquid; then spheres were picked according to Eq. (3.7) and availability in the market as listed in Table 2. The $\frac{1}{8}$ -in tungsten carbide, $\frac{1}{4}$ -in steel, $\frac{7}{16}$ -in ceramic and $\frac{5}{8}$ -in aluminum spheres were used to test size effects, and $\frac{1}{4}$ -in teflon, aluminum, steel and tungsten carbide spheres were used to test weight (or velocity) effects on attraction and dispersion.

4. Interactions between spheres falling side-by-side

We dropped two spheres side-by-side in a channel filled with different liquids. In viscoelastic liquids, when the initial separation distance is small, the two spheres will attract; the line between centers will turn as they attract, until the spheres touch and chain with the line of centers vertical. Close side-by-side settling at slow speeds is unstable in viscoelastic fluids and the dynamics creates stable vertical chains. The tilting of the line of centers between falling spheres starts at the instant of release and the two spheres appear as a dumbbell pair sliding along the tilting line of centers as in Fig. 10(a).

If the initial distance is large enough, the two spheres appear not to interact and to fall straight down as in Fig. 10(c). Sphere–sphere interactions in this regime are not strong. We shall call this regime “non-interacting” though we recognize that

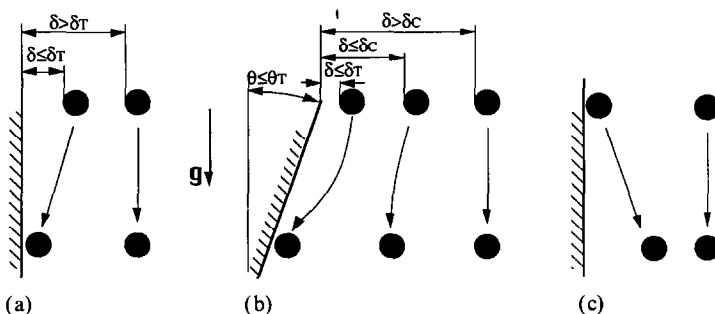
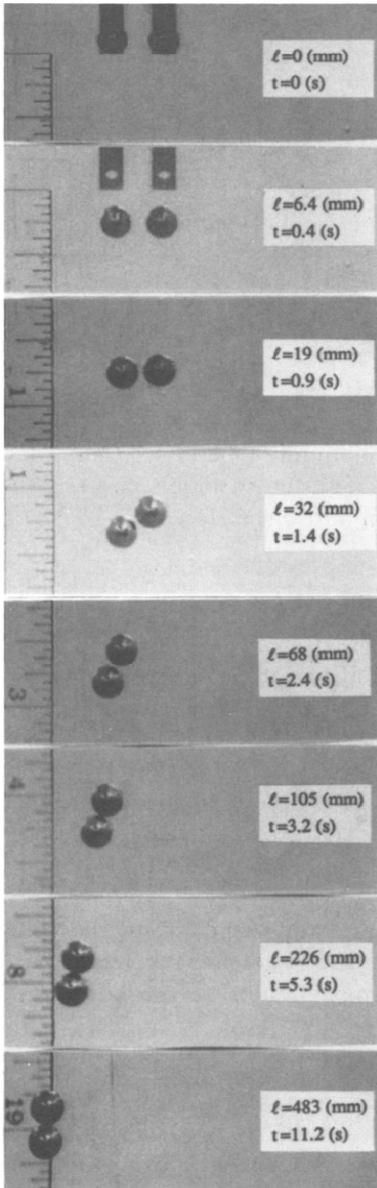
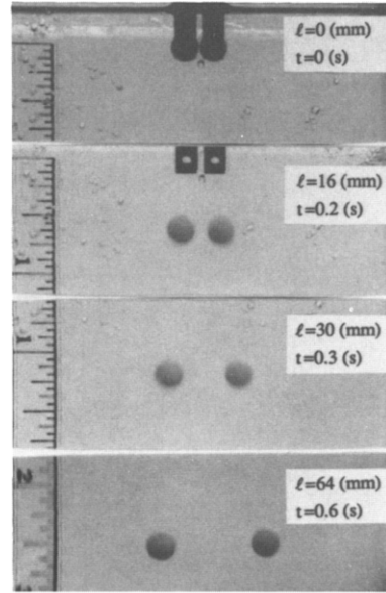


Fig. 10. (a)–(c). Continued on next page.



(d)



(e)

Fig. 10. (a) Settling spheres in a viscoelastic liquid when $\delta (\leq \delta_T)$ is small; (b) settling spheres in a Newtonian liquid when δ is small; (c) settling spheres in any liquid when δ is large; (d) $\frac{1}{4}$ -in steel spheres falling in 1.5% aqueous polyox, initial distance $\delta = 3.84$ mm, l is the vertical distance from the point of release to the mid-point on the line of centers; (e) $\frac{1}{4}$ -in teflon spheres falling in 50/50 glycerin–water solution. Two spheres released side-by-side at the same time in a viscoelastic fluid with $\delta < \delta_T$ will attract each other while the line of centers between the spheres rotates towards the vertical (as in (d)). The final result is a vertical chain of two spheres (a). If $\delta > \delta_C$, then the spheres appear not to attract (c). If $\delta_T < \delta < \delta_C$, the spheres attract initially and the line of centers between spheres will turn from the horizontal but the spheres eventually separate, or stop interacting and never touch or chain. In a Newtonian liquid, two spheres dropped side-by-side with a small gap or not gap will disperse rather than aggregate (b). If the initial distance between two spheres is large enough, then they apparently will fall without interaction. Some photographs from experiments are shown in (d) and (e).

some small interactions that could produce a large effect over long time periods are probably at work.

In Newtonian fluids, two spheres launched side-by-side, which are initially separated by a small gap or no gap, will separate as in Fig. 10(b). If the initial gap is large enough the two spheres enter into the non-interacting regime described in

the preceding paragraph and in Fig. 10(c). Side-by-side sedimentation is relatively stable or only weakly unstable and spheres will never chain in Newtonian liquids.

Two heavy spheres falling faster than the wave speed for the fluid in a viscoelastic fluid will disperse as in a Newtonian fluid. This phenomenon is the same one that causes long bodies that fall straight down at slow speeds to turn 90° into broadside-across-the-stream fall at supercritical speed when inertia dominates viscoelasticity [1,2].

Returning now to the fall of spheres launched side-by-side in the strongly subcritical case, we look at a range of initial separation distances that are larger than those for which chaining occurs and smaller than those for which the falling spheres apparently do not interact. The dynamics of aggregation and dispersion here is more complicated. Two spheres will attract initially and the line of centers between them turns toward the vertical. The spheres do not touch but instead, enter into a non-interacting regime, or else actually separate in a manner reminiscent of the settling behavior of distant spheres, with the line of centers vertical, that was studied by Riddle et al. [15]. This behavior is illustrated in Section 4.1. The two spheres attract initially, but they do not come into touching contact and eventually separate.

Now we are prepared to define two distinct distances. The first distance δ_C is the largest side-by-side distance δ for which attraction can be observed, as shown in Fig. 10. This critical distance may not be a precisely defined value; it may depend on the level of resolution of the measurement of the mutual attraction that we can achieve in our experiment. If $\delta \leq \delta_C$ the spheres will attract initially. For small $\delta \leq \delta_C$ the line of centers between spheres will turn from the horizontal and the spheres will attract, touch and then fall in a chain with line of centers vertical. For large values of $\delta \leq \delta_C$ the spheres attract initially and the line of centers between spheres will turn from the horizontal but the spheres eventually separate, or stop interacting and never touch or chain. We did not try to measure δ_C . The set of small $\delta \leq \delta_T$ for which falling side-by-side spheres eventually touch is defined by a second distance $\delta_T < \delta_C$, called the critical touching distance. δ_T is determined by observations associated with measurements. We increased the initial separation distance by small steps and repeated experiments a few times under each condition. The vertical distance between release and the point of touching is called the vertical touching distance $l_T(\delta)$ (Fig. 10(a)).

Table 3 lists measured values of the fall velocity U and the shear rate $\dot{\gamma} = U/D$. The Reynolds number Re_0 and Weissenberg number W_0 are zero shear values (2.12) and (2.13).

Table 4 lists the vertical distance $l_T(\delta)$ traveled by spheres before touching (Fig. 10) as a function of the initial distance δ between the spheres.

The lateral migration of spheres depends on the fall velocity, which is determined by the weight of sphere, as well as on the properties of the fluid in the settling bed. Effects of the weight of the particles can be assessed to a degree by normalizing all the lengths with the lateral touching distance δ_T which also depends on the weight. Figure 11 shows that heavier particles achieve larger fall distance ratios l_T/δ_T for a given initial distance fraction δ/δ_T . The effect of the weight of particles is weak. $\frac{1}{4}$ -in tungsten, steel and teflon spheres have very different weights (Table 2) and fall

Table 3
Measured values of the fall velocity and related quantities

Liquid–solid	U (cm s ⁻¹)	$\dot{\gamma}$ (s ⁻¹)	Re_0	W_0
1.25% polyox– $\frac{1}{4}$ -in. steel	6.34	9.98	0.032	4.29
1.5% polyox– $\frac{1}{4}$ -in. steel	3.08	4.85	0.011	2.04
STP– $\frac{1}{4}$ -in. steel	0.37	0.58	0.001	0.001
S1– $\frac{1}{4}$ -in. steel	0.99	1.56	0.008	0.028
S1– $\frac{1}{4}$ -in. tungsten	2.11	3.32	0.017	0.058
S1– $\frac{1}{4}$ -in. teflon	0.11	0.17	0.001	0.003
Xanthan– $\frac{1}{4}$ -in. teflon	10.9	17.2	0.133	6.01
Carbopol– $\frac{1}{4}$ -in. teflon	4.99	7.86	0.417	0.209

Table 4
Attraction between side-by-side spheres in different liquid–solid systems

Liquid–solid	Initial distance δ (mm)	Vertical distance l_T from releasing to touching (mm)	Critical touching distance δ_T (mm)
0.3% aqueous Xanthan–teflon	2.5	57	6
	5	79	
0.4% Carbopol in 50/50 glycerin–water–teflon			No attraction
STP–steel	1.3	60	11
	2.5	120	
	3.8	290	
	5.1	470	
	6.4	590	
S1–steel	2.5	23	17.5
	5.1	61	
	7.6	130	
	10.2	225	
	11.4	300	
S1–tungsten	3.8	100	15
	7.6	300	
S1–teflon	3.8	75	5
1.5% aqueous polyox–steel	1.3	9.5	5
	2.5	51	
	3.3	68	
	3.8	89	
	4.1	102	
1.25% aqueous polyox–steel	1	12	8
	2	21	
	3	74	
	4	90	
	5	108	
	5.8	114	
	7.1	150	

The vertical distance $l_T(\delta)$ traveled before touching depends on the ratio of the fall velocity to the lateral migration velocity.

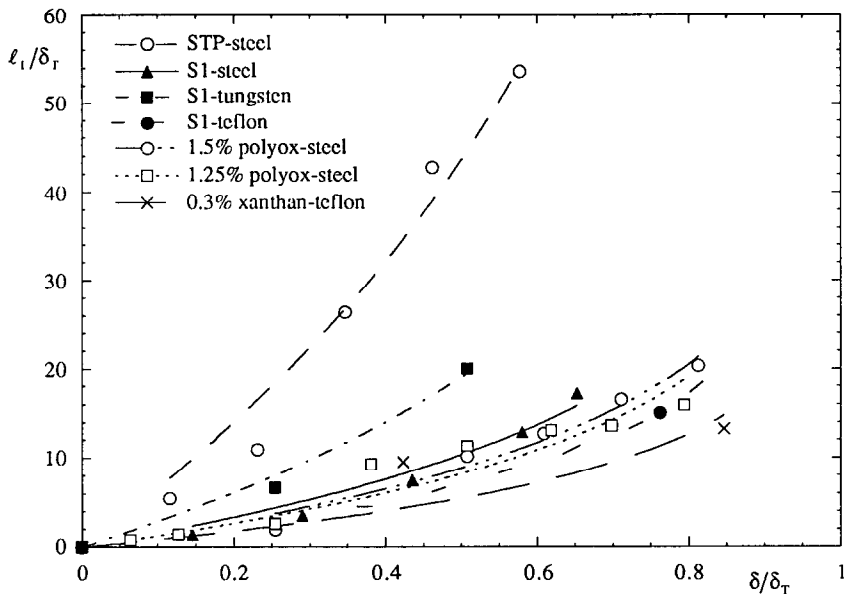


Fig. 11. Interaction between side-by-side sedimenting spheres in different fluids in terms of the ratio ℓ_1/δ_T of vertical distance traveled by the sphere before touching over the critical touching distance as a function of the ratio δ/δ_T . Full symbols refer to S1 and empty circles to STP.

speeds in S1 (Table 3), but the ratio of the lateral drift distance to the vertical touching distance is not very great. The weak affects of weight are more easily seen in experiments, discussed in Sections 6 and 7, in which spheres are attracted to a vertical wall. We do not mean to imply that weight effects are generally not important, but only to note the tendency of the lateral drift velocity to increase in proportion to the fall velocity.

It is of interest to examine data for steel particles. The data for steel in Fig. 11 order weakly with the elastic stress ratio coefficient $10\beta/3\eta_0$ in Table 1, with strength of interaction for steel in different fluids in the order: STP, S1, 1.5% polyox and 1.25% polyox. The data for teflon are too sparse for us to draw a definite conclusion. Xanthan which is strongly shear-thinning and has a zero elastic stress coefficient, does not seem to be greatly different than S1, which does not shear-thin at the small shear rate of 0.17 of our experiments (see Table 3).

4.1. Interaction in aqueous polyox solutions

In Fig. 12 the distance between two $\frac{1}{4}$ -in falling spheres dropped side-by-side are shown as a function of the vertical distance from the point of release. Four different values of δ are considered. Attraction between the particles is stronger and particles aggregate at a smaller distance from the point of release when the initial side-by-side distance δ is small. If δ is large, falling spheres will not touch. In this figure, the triangles illustrate the behavior, mentioned above, of sphere separation.

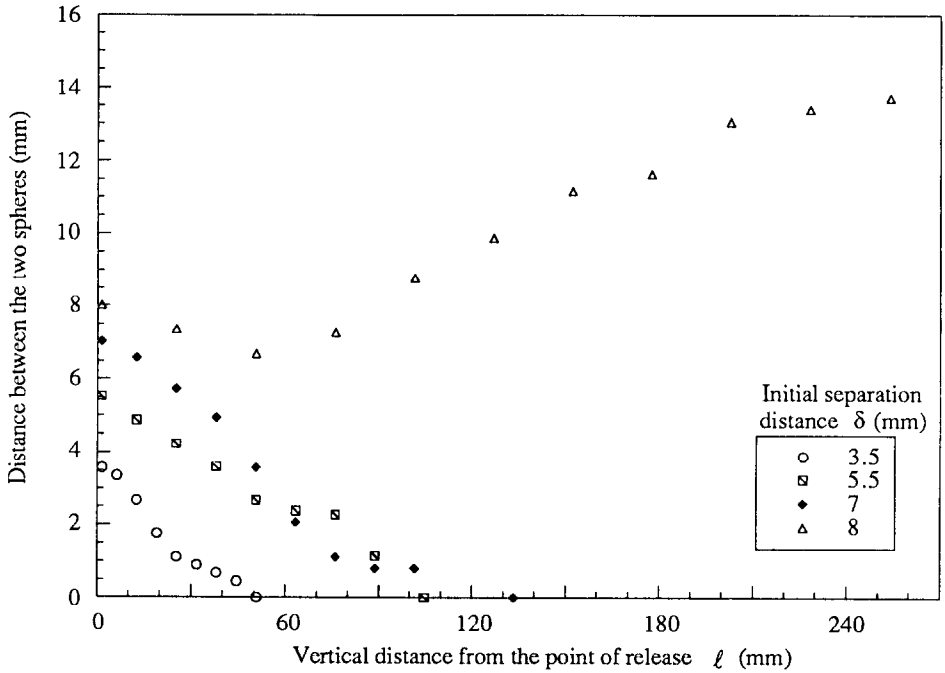


Fig. 12. Separation distance between spheres measured along the line of centers vs. the vertical distance l to the mid-point between the spheres in 1.25% polyox solution.

The vertical distance $l_T(\delta)$ traveled by $\frac{1}{4}$ -in steel spheres before touching vs. the initial distance δ between the spheres is plotted in Fig. 13(a) and 13(b). Spheres falling in 1.25% aqueous polyox solution did not touch when $\delta > \delta_T \approx 8$ mm and $\delta_T \approx 5$ mm in 1.5% aqueous solution. Values of flow parameters for the experiments shown in Fig. 13 are listed in Table 3.

We were at first surprised to find that the critical touching distance was greater in the 1.25% polyox solution than in the 1.5% solution. This unexpected result perhaps finds its explanation in the fact that the stress ratio N_1/τ (Table 1) is actually larger in the more dilute solutions, indicating a sense in which the dilute solution is actually more elastic. Consequently, we would predict even stronger interaction in the 1.0% than in the 1.25% solution.

Clusters of spheres dropped together in the polyox solution will form streamline arrays (see Fig. 14). Chains of spheres, like long bodies, tilt their longside parallel to streamlines. Their falling speeds are less than the shear wave speeds in these cases.

4.2. Interaction in S1 and STP

Pairs of steel spheres were released in STP. Pairs of steel, tungsten and teflon spheres were released in S1. The behavior of attracting spheres in this experiment

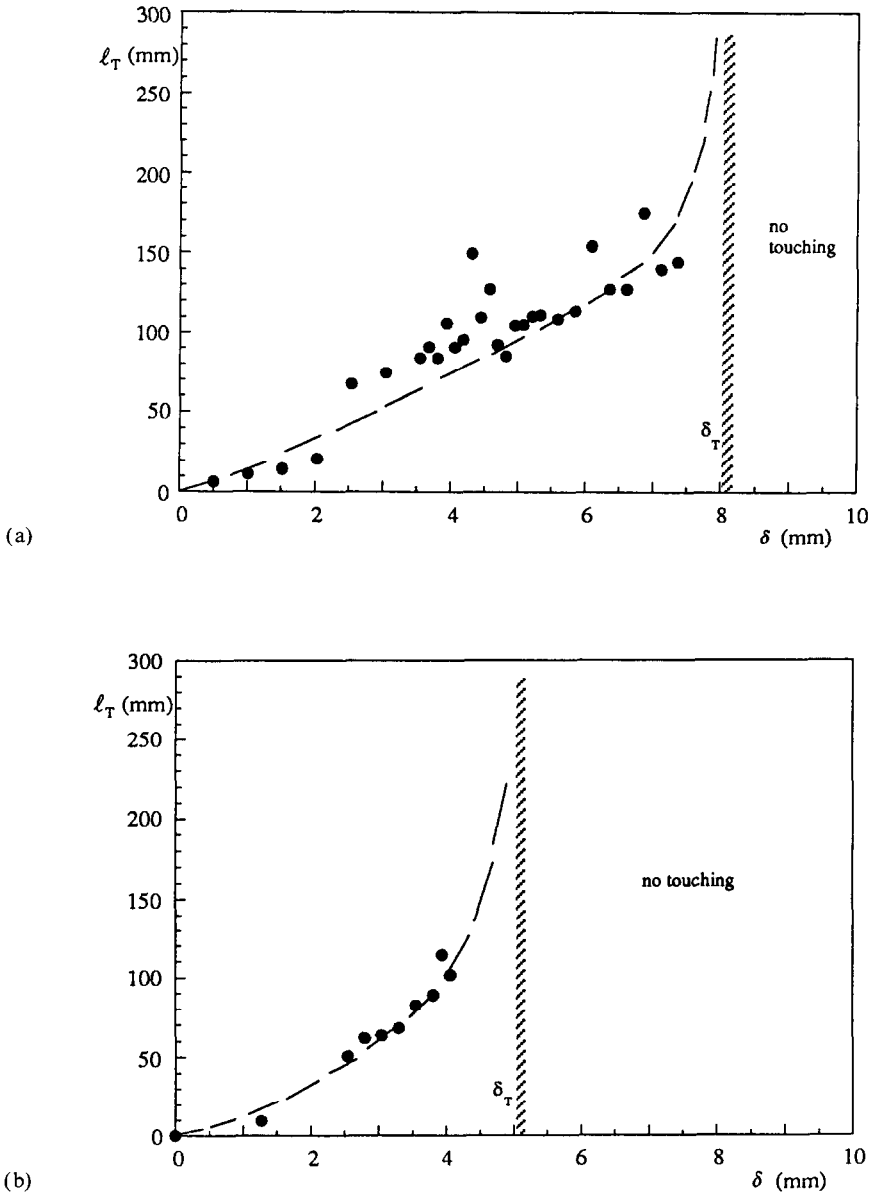


Fig. 13. $l_T(\delta)$ vs. δ for $\frac{1}{4}$ -in steel spheres in: (a) 1.25% aqueous polyox solution; (b) 1.5% aqueous polyox solution. The critical touching distance is larger in the 1.25% solution.

was qualitatively similar to that described in the previous section. The critical touching distance in STP is about 11 mm. This is smaller than the critical touching distance of 17.5 mm in S1. The elastic ratio of the first normal stress to the shear stress at small rates of shear is an order of magnitude larger in S1 than in STP

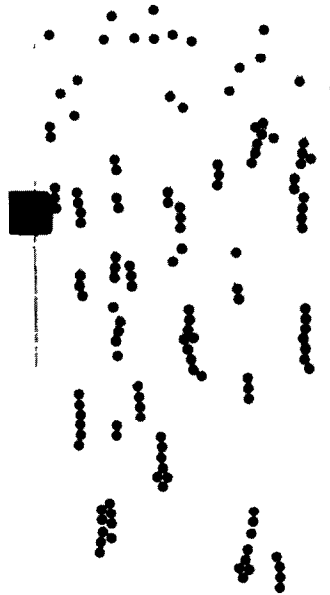


Fig. 14. Chains of $\frac{1}{4}$ -in steel spheres falling in 1.25% aqueous polyox solution. The same kind of chaining was observed in the 1.5% aqueous polyox solution.

(Table 1). The experimental results are presented in detail in Tables 3 and 4, and Fig. 11. Fig. 15 shows chains of spheres falling in S1 and STP.

4.3. Interaction in Xanthan and Carbopol

Experimental results for side-by-side attraction in all liquid–solid systems including Xanthan and Carbopol are given in Table 4. Two spheres dropped side-by-side do attract in 0.3% aqueous Xanthan solution, but the attraction is weak. The critical touching distance of teflon spheres is about 6 mm. There is no attraction in 0.4% Carbopol in 50/50 glycerin–water solution. Two spheres dropped closely side-by-side will separate as in a Newtonian liquid. The flow parameters are given in Table 3. The chains of spheres falling in these two liquids are shown in Fig. 16.

In comparing the results we have obtained in our experiments with different liquids, we see a definite difference between side-by-side attraction and the chaining spheres. In this tentative and preliminary interpretation of our results we focus on the effects of normal stresses and shear-thinning with and without memory. STP and S1 are basically non-shear-thinning at the low rates of shear characteristic of our experiments. Side-by-side spheres attract in these fluids and they also chain, indicating that shear-thinning is not a necessary condition for these effects. S1 is a more mobile and elastic fluid than STP and it gives rise to stronger attraction and

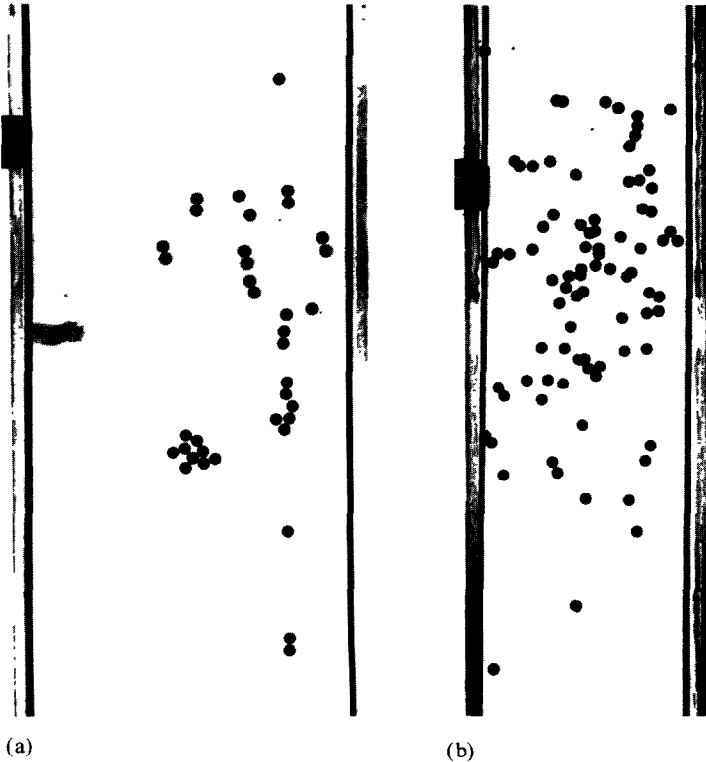


Fig. 15. Chains of $\frac{1}{4}$ -in steel spheres falling in (a) S1 and (b) STP.

chaining. This suggests that fluids for which the elastic ratio of normal stress effects to viscous effects is large will give rise to strong interparticle forces, attraction and chaining. The polyox solutions have large elastic normal stresses, elastic stress ratios and times of relaxation as well, but they also shear-thin strongly at shear rates characteristic of our experiments. Although the presence of all the viscoelastic effects in polyox solutions does not allow us to isolate the properties of a viscoelastic fluid that give rise to the strong particle interactions that we observed in our experiments, these interactions also appear to correlate large values of the stress ratio well. The correlation in polyox is subtle because the less concentrated solutions have higher stress ratio and stronger interactions.

To isolate the effects of shear-thinning we looked at the Xanthan and Carbopol solutions, which do not give measureable values of normal stresses at any rate of shear. The value of the elastic stress ratio may be large in Xanthan, but the ratio cannot be determined because the normal stresses are too small to measure. However, the 0.3% aqueous Xanthan has a much higher linear elasticity than Carbopol. We are assuming that this means that the memory of shear-thinning is much longer in Xanthan. In fact the Xanthan will exhibit side-by-side attraction weakly and chain strongly, but the 0.4% Carbopol does neither.

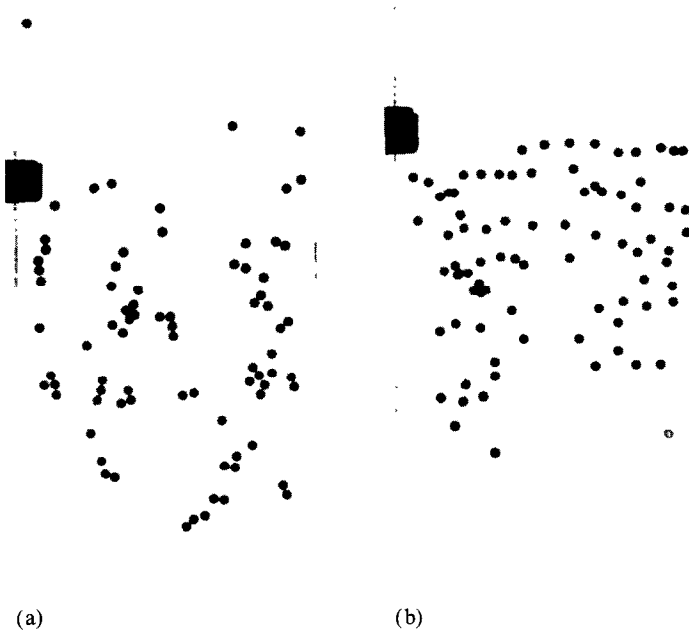


Fig. 16. Chains of $\frac{1}{4}$ -in teflon spheres falling in (a) 0.3% aqueous Xanthan and (b) 0.4% Carbopol in 50/50 glycerin–water solution. Horizontal arrays of spheres are relatively stable in the Carbopol solution and vertical arrays are relatively stable in the Xanthan solution.

Our experiments show that different mechanisms promote aggregation in viscoelastic liquids; more than one property is involved. A possible generalization of our observations is that large values of the elastic stress ratio N_1/τ are sufficient but not necessary for strong interactions. Shear-thinning plus memory, which creates corridors of reduced viscosity, is also sufficient but not necessary for strong interactions. Aggregation seems not to occur in inelastic fluids with short memory or small values of N_1/τ , whether or not they shear-thin.

5. Direct two-dimensional simulation of the interactions between two particles falling side-by-side in Newtonian fluids

The hydrodynamic mechanisms that cause circular particles to rotate and drift away from each other in a Newtonian fluid can be understood by direct (two-dimensional) numerical simulation, using the Navier–Stokes equations to find the fluid motion and hydrodynamic forces which move the rigid particles according to Newton’s equation of motion. A finite element package based on POLYFLOW with this capacity has been presented by Hu et al. [29], and a video of this simulation together with a short paper has been given by Hu et al. [30]. Huang et al. [31] applied this code to study the forces and the turning couple on an elliptic particle settling in a vertical channel, and they showed that there is high pressure on

the front side of the ellipse at the place where the shear stress vanishes, which corresponds to a stagnation point in potential flow. This pressure acts always to keep the long side of the body perpendicular to the fall. Feng et al. [32] used this code to solve initial value problems for circular particles settling in a channel and this section is an adaptation of their work to the problem at hand. An analysis like this one has been applied by Liu et al. [12] to the problem of interaction between a circular particle falling in a Newtonian fluid and a vertical wall.

We want to understand how two heavier-than-liquid circular particles dropped side-by-side from rest in a channel will rotate and move. Referring to Feng et al. [32] for details, we note here that in the regimes of moderately low Reynolds numbers in which there is no vortex shedding, the particles will commence to rotate as if turned by the shears from the fluid going around the outside of the particle and not from the fluid in the gap. As the particles acquire angular velocity, they separate and fall side-by-side for a time before they enter into a staggered arrangement. The side-by-side walls of the channel are important, especially in the later stages of the motion.

In our experiments, spheres dropped side-by-side in Newtonian liquids would begin to rotate and drift rapidly away from each other and after a short time reach an apparently steady state with definite angular velocity and a fixed stand-away distance with no further drift. In this simulation, a fixed stand-away distance with the line of centers perpendicular to the flow is not achieved. The side-by-side configuration, however, is very persistent as Fig. 17 shows.

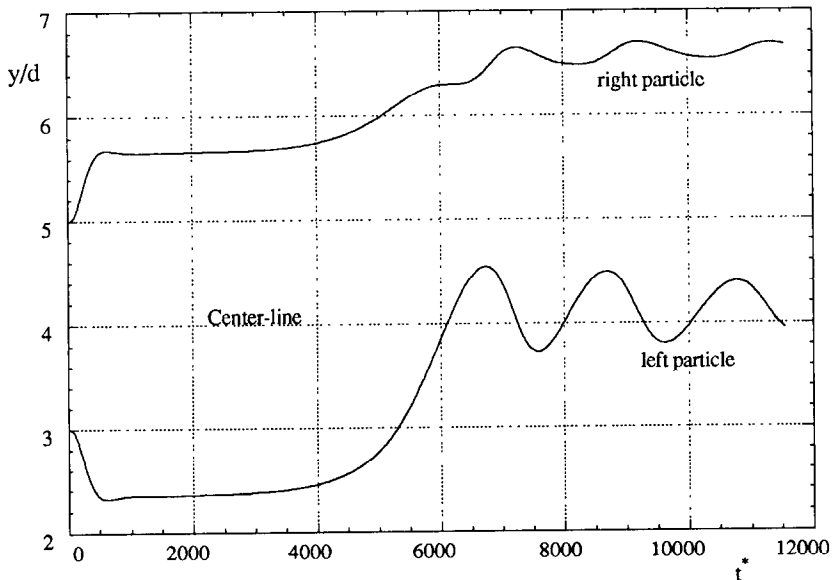


Fig. 17. Trajectories of two circular cylinders dropped from a side-by-side initial condition in a channel of 8-diameter width. The dimensionless time is defined by $t^* = t\sqrt{g/d}$. The oscillation seen in the trajectories is associated with a wall effect.

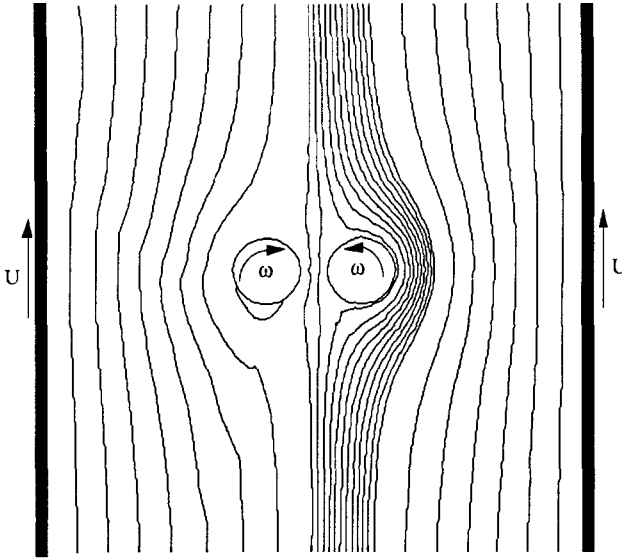


Fig. 18. Streamlines for side-by-side sedimentation of two circular particles dropped from rest in an 8-diameter channel. The particles are at an early stage of sedimentation ($t^* = 31$ in Fig. 17). To visualize the streamlines, we use a coordinate system fixed at the center of the right particle, which is moving down and to the right side. In this system, the centerline between the particles is not a streamline.

At first, when the side-by-side particles are close together, the passage of fluid between them is blocked, so that the flow passes over the outside of the particle, turning them as in Fig. 18. We are going to show that the pressure and the shear stress distributions on the surface of the particle give rise to a lateral force and a torque that define the drift and rotation of the particles.

Fig. 19 shows that the maximum pressure occurs near $\theta = 202.5^\circ$. This position is also where the dividing streamline seems to hit the surface of the body in Fig. 18. Because the circular particle is rotating, the no-slip condition implies that there are closed streamlines around the surface of the particle and a stagnation point cannot be strictly defined. But considering the outside streamlines, we shall call the point with maximum pressure a viscous stagnation point. We have shown that the stagnation point usually corresponds to vanishing shear stress [12,31]. This is not the case here because of the strong rotation of the particle. If we modify the shear stress by taking out the contribution from rotation, we should still have the correspondence. This is done by considering a potential vortex at the center of the particle with velocity

$$u_\theta^p = \omega a^2 / r, \quad (5.1)$$

where ω is the angular velocity at this moment. The shear stress at $r = a$ for this is

$$\tau_{r\theta}^p = -2\eta\omega. \quad (5.2)$$

After removing the shear stress (5.2), we obtain the effective shear stress in Fig. 19. Thus, the maximum pressure occurs at the stagnation point where the effective

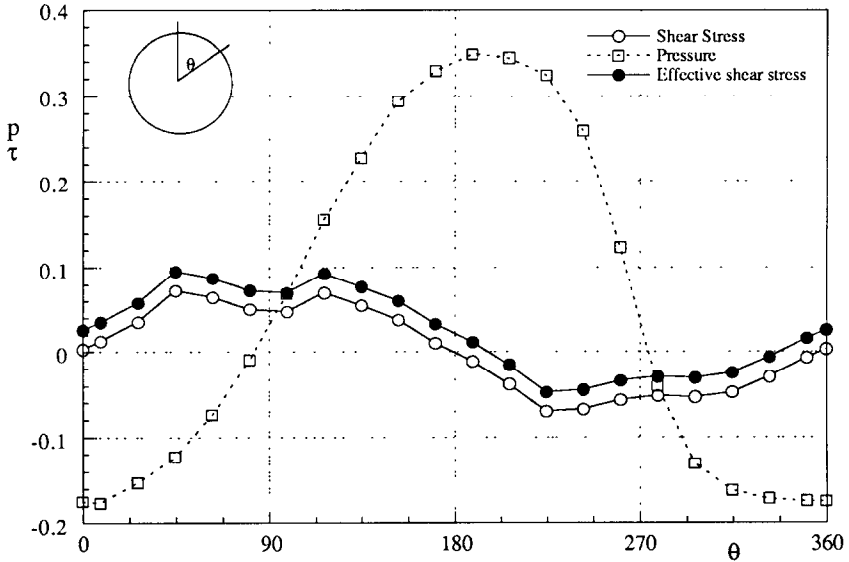


Fig. 19. The pressure and shear stress distribution on the surface of the right particle. Dimensionless time $t^* = 31$, and instantaneous Reynolds number $Re = 2.65$.

shear stress vanishes. We also tested a particle prevented from rotation and settling at virtually the same Reynolds number. The distributions of pressure and viscous stresses are shown in Fig. 20. The shear stress distribution is very much like the

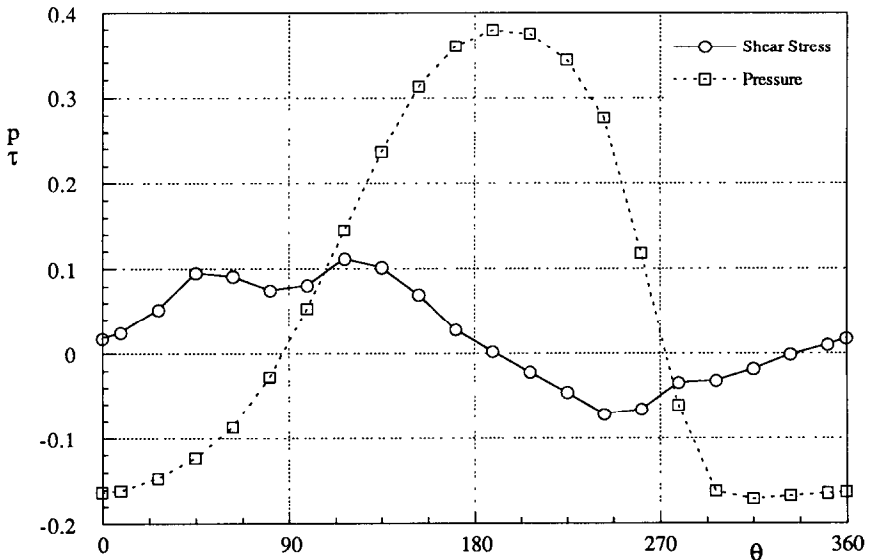


Fig. 20. The pressure and shear stress distributions on the right particle. The particles are prevented from rotation. Dimensionless time $t^* = 30$, instantaneous Reynolds number $Re = 2.76$.

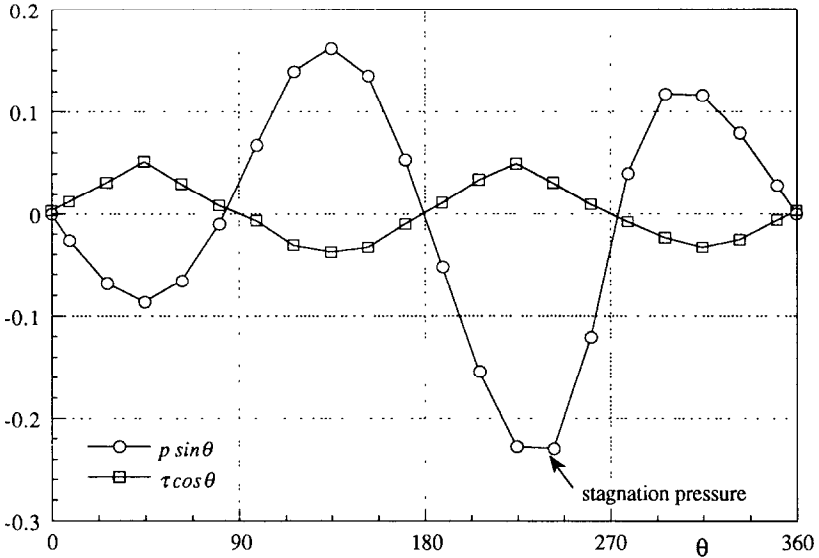


Fig. 21. The horizontal component of the pressure and shear stress shown in Fig. 19. Because of the definition of θ , negative lateral thrusts point to the right.

modified shear stress in Fig. 19, and the zero of the shear stress is the viscous stagnation point that locates the pressure maximum.

Figure 21 shows that the stagnation pressure controls on the sidewise drift, increasing the distance between repelling particles. In this figure we have compared the side thrusts, $p \sin \theta$ of the pressure and $\tau \cos \theta$ of the shear stress on the surface of the particle. The resultant forces are

$$[F_p, F_\tau] = \int_0^{2\pi} [p \sin \theta, \tau \cos \theta] a \, d\theta = (1.602 \times 10^{-3}, 8.034 \times 10^{-4}) \text{ dyn cm}^{-1}. \quad (5.3)$$

The pressure force is larger than the shear stress force, and the separation of the two particles is therefore determined mainly by the stagnation pressure.

The rotation of the particle is associated with the fact that the positive shear stress on the right side is larger than the negative shear stress on the left. This is even clearer in the case of non-rotating particles shown in Fig. 20.

6. The interaction between a wall and a settling sphere

If a sphere is released at a small distance from a vertical wall in a viscoelastic fluid it will eventually approach the wall and fall while rolling up along the wall (anomalous rolling is discussed by Joseph et al. [11] and Liu et al. [12], see Fig. 22(a)). Even when the wall is slightly tilted away from gravity, the wall will attract a sedimenting sphere that is dropped near the wall. On the other hand if δ is large

the sphere and wall do not appear to interact during the short fall time of our experiments (Fig. 22(b)).

Spheres dropped at or near a vertical wall in a Newtonian fluid will be repelled by the wall (Fig. 22(c)), just the opposite of what occurs in a viscoelastic fluid. Spheres that are sufficiently far from the wall initially do not appear to interact. The results of a direct two-dimensional numerical simulation of a circular particle falling near a vertical wall in a Newtonian fluid was given by Liu et al. [12].

Returning to the case of viscoelastic fluids near a tilted wall, we may define two critical values δ_C and δ_T , the critical distance of interaction and the critical touching

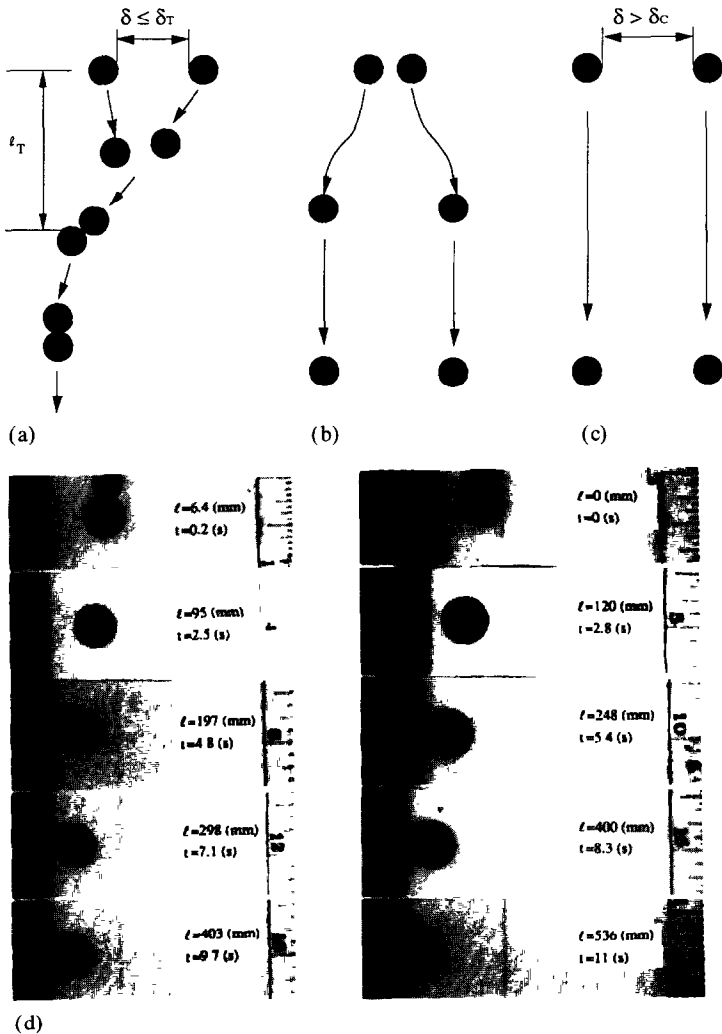


Fig. 22. (a)–(d). Continued on next page.

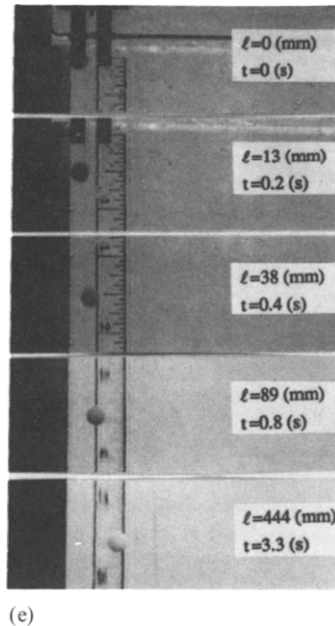


Fig. 22. (a) Settling of spheres in viscoelastic liquid near a vertical wall; (b) settling of spheres in viscoelastic liquid near a tilted wall; (c) settling of spheres in Newtonian liquid near a vertical wall; (d) a $\frac{7}{16}$ -in ceramic sphere falling near a vertical wall (left, $\delta = 10$ mm) or a 1° tilted wall (right, $\delta = 5$ mm) in 1.5% aqueous polyox solution; (e) a $\frac{1}{4}$ -in teflon sphere falling near a vertical wall in 50/50 glycerin–water solution. A sphere released in a viscoelastic liquid will be attracted to the wall when the initial distance δ of the sphere from the vertical wall (a) or the tilted wall (b) is smaller than the critical touching distance δ_T ; but will fall straight down when $\delta > \delta_T$ in (a) and $\delta > \delta_C$ in (b). In case (b) with the wall slightly tilted with $\theta \leq \theta_T$, when $\delta_T < \delta < \delta_C$, a sphere will experience some wall attraction but will not migrate all the way to the wall and will eventually fall straight down. In Newtonian liquids, a sphere dropped at a small distance or no distance from the wall will migrate away from the wall (c).

distance respectively, with $\delta_T \leq \delta_C$ as in the case of the interacting pairs of spheres. If $\delta < \delta_T$, then the sphere eventually migrates nearly all the way to the wall and never falls away. Usually, the gap between the sphere and the wall is too small to measure easily. If $\delta_T < \delta < \delta_C$, the sphere will move toward the wall, but it will eventually fall away (Fig. 22(b)). In our experiments, spheres were dropped at increasing distances from the top corner of the tilted rod, at different angles of inclination of the rod between 0 and 5° . There is a critical tilt angle θ_T such that when $\theta > \theta_T$, spheres are not attracted all the way to the wall.

6.1. Vertical wall

Sphere trajectories are shown in Fig. 23 for $\frac{1}{4}$ -in. steel spheres dropped in 1.5% polyox at different initial distances from a vertical wall ranging from 2 to 12 mm. These trajectories are approximately straight lines suggesting that the ratio of the fall velocity to the lateral migration velocity is constant. The free fall terminal

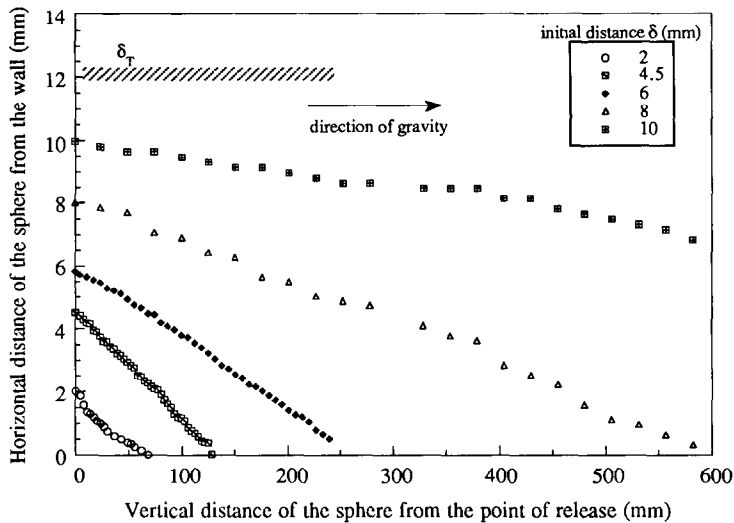


Fig. 23. Distance between a falling sphere and a vertical wall in 1.5% polyox as a function of the vertical distance of the spheres from the point of release.

velocity was reached at a distance of about 5 cm from the release point by those particles that had not touched the wall. Spheres starting at smaller initial distances δ migrate to the wall more rapidly. For larger initial distances, attraction between the falling sphere and the wall could not be observed in the time it takes for a particle to fall to the bottom of the channel. $\delta = \delta_T$ is an effective critical distance such that when $\delta > \delta_T$ the sphere is apparently not attracted by the wall. Figures 24(a) and 24(b) plot the vertical distance traveled by the sphere before touching the wall as a function of the initial distance between the sphere and the wall for 1.25% and 1.5% polyox solutions. The open circles in Fig. 24 are for values of l_T longer than our channel which was extrapolated from particle trajectories. The 1.25% solution, which has a higher elastic stress ratio N_1/τ than the 1.5% solution (see Table 1), also has a larger δ_T .

It is of interest to compare the critical values of δ for a plane wall with a sphere and for two spheres launched side-by-side. The attracting or repelling power of a wall is larger than that between two spheres, because the wall can be visualized as a vertical array of touching spheres. Each sphere in the array attracts or repels the free test sphere, but with a different power of interaction depending on the variable distance between the spheres. So the interaction power of a wall is obtained by integration of the interaction of each small part of it. Reasoning in this way we would think that a wall could attract a free particle in a viscoelastic fluid at a much greater power than a single sphere could do. In fact, because the wall would not move by interaction with the free particle, we should actually define the critical touching distance $(\delta_T)_{WS}$, in the case of wall–sphere interaction, as twice the distance between the sphere and the wall, i.e., the distance between the sphere and its image with respect to the wall. Comparing $(\delta_T)_{WS}$ with $(\delta_T)_{SS}$, which is the

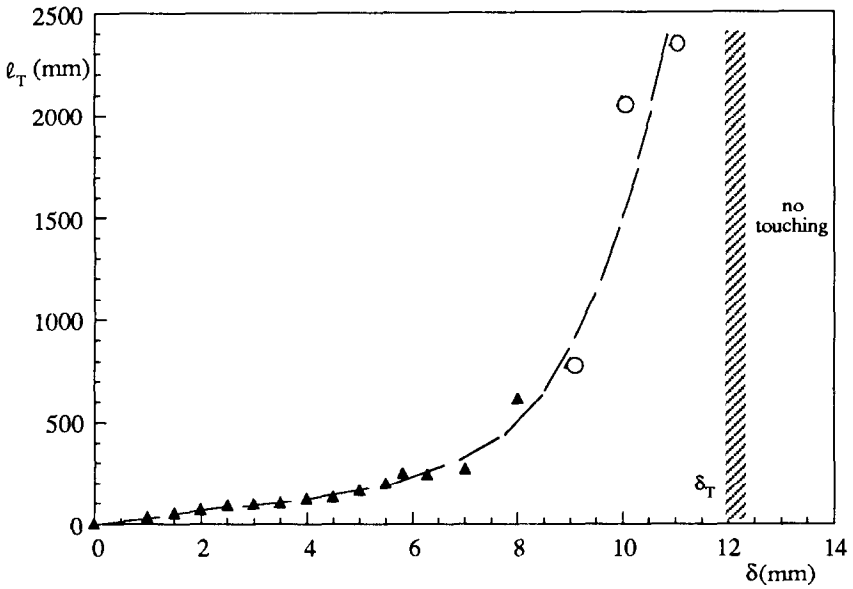
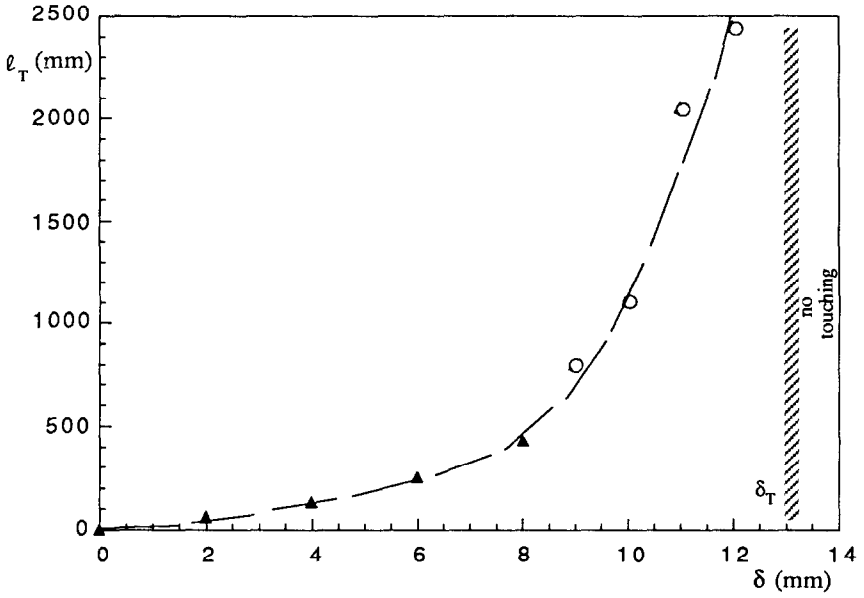


Fig. 24. Interaction between a falling sphere (steel, $\frac{1}{4}$ -in diameter) and a vertical wall in terms of the vertical distance l_T traveled by the sphere before touching the wall as a function of the initial separation distance δ between the sphere and the wall: (a) 1.25% polyox solution; (b) 1.5% polyox solution.

Table 5
Comparison of critical values between wall–sphere and sphere–sphere interactions

Liquid–solid	$(\delta_T)_{ss}$	$(\delta_T)_{ws}$
Polyox 1.25%–steel	8	26
Polyox 1.5%–steel	5	24
S1–steel	17.5	24
S1–tungsten	15	20
S1–teflon	5	6
STP–steel	11	—
Xanthan–teflon	6	6

critical touching distance for falling spheres launched side-by-side, we see from Table 5 that $(\delta_T)_{ws}/(\delta_T)_{ss} = 1 \approx 4$ for all the liquids that show attraction except STP. The falling velocity is slowest in STP so the lateral migration velocity may also be too small to produce a noticeable effect in channels as short as those used in our experiments. In a Newtonian fluid, the wall will force the test particle to move out further than spheres settling side-by-side. In the experiments in which $\frac{1}{4}$ -in teflon spheres fall in a 50/50 glycerin–water solution, twice the distance between the sphere and the wall is ultimately 1.7 times greater than the distance between two spheres.

6.2. Tilted wall

The case of an inclined wall is more complex. The settling sphere can move toward the wall initially and then fall away. In Fig. 25, we have plotted trajectories of a 14-in. steel sphere falling near a 1.5° tilted wall for different initial distance in a 1.5% aqueous polyox solution. We can identify a first critical distance, critical touching distance δ_T , that separates the initial distances for which spheres appear to touch the wall eventually from those for which they will not touch. As in the case of attracting spheres, we were able to identify a second critical distance δ_C . When $\delta < \delta_C$ the sphere will move toward the wall initially, but it may not reach the wall. When $\delta > \delta_C$ no attraction was observed. In Fig. 26, we have plotted δ_T and δ_C as a function of the tilt angle for 1.25% polyox solution (Fig. 26(a)) and for 1.5% polyox solution (Fig. 26(b)). From this figure we see that δ_T and δ_C decrease with increasing tilt angle.

Table 6 lists critical touching distances δ_T and critical interaction distances δ_C for $\frac{1}{4}$ -in. spheres of different weights falling in various fluids. Spheres falling near vertical and tilted walls in STP or Carbopol are not attracted to the wall. STP has normal stresses but does not shear-thin. Carbopol shear-thins but has no measurable normal stress. On the other hand, the wall attracts spheres in the shear-thinning Xanthan, which also has no measurable normal stresses, but has much longer memory than Carbopol. Sphere–wall interactions are stronger in S1 and polyox solutions. We do not yet understand the mechanisms that control lateral migration.

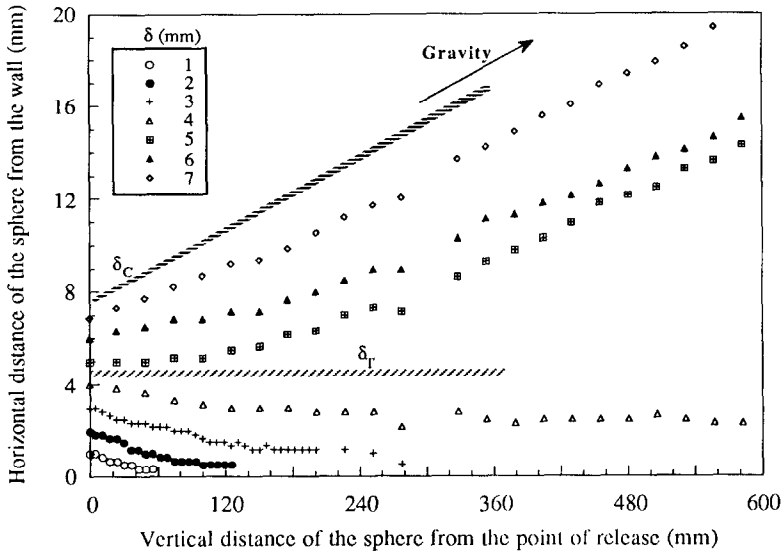


Fig. 25. Trajectories of a $\frac{1}{4}$ -in steel sphere falling near a wall tilted 1.5° from the vertical in a 1.5% aqueous polyox solution. The plane is divided into three regions $\delta < \delta_T$, $\delta_T < \delta < \delta_C$ and $\delta > \delta_C$. The arrow shows the slope of the trajectory a particle would have if it fell vertically.

Spheres with different weights (Table 2) were dropped in S1. The results show that the effect of particle weight on δ_T is the same as in the case of side-by-side settling of spheres (see Table 4).

6.3. Effects of sphere size and weight

These experiments were done later than the others and we used a fresh 1.5% aqueous polyox solution as a test liquid. The graphs of viscosity and the dynamic moduli of this solution as functions of shear rate or frequency are similar to those shown in Figs. 1 and 2. The parameters, listed in Table 1, for this solution are as follows: $\eta_0 = 10.6 \text{ Pa s}$, $\kappa = 4.67$, $n = 0.46$, $\beta = 1.44 \text{ g s}^{-1}$, $\psi_{10} = 480 \text{ g s}^{-1}$, $c = 23.0 \text{ cm s}^{-1}$, $\lambda_0 = 0.20$, $\psi_{10}/\eta_0 = 10\hat{\beta}/3\eta_0 = 4.52 \text{ s}$. The flow parameters of the experiments are listed in Table 7.

Figure 27 shows the interactions between falling spheres and a vertical wall in terms of the vertical distance traveled by the sphere before touching the wall as a function of the initial distance between the sphere and the wall. It can be seen from Fig. 27(a) that the particle weight does not have an obvious effect on attraction between a sphere and a vertical wall. All the tested spheres of the same size but different weight have about the same critical distances. For a given initial separation distance δ each of the four different spheres travels approximately the same distance in the vertical direction before touching the wall; $l_T(\delta)$ does not depend strongly on weight. However, the size of the sphere has an effect on the attraction. This effect is shown in Fig. 27(b). The larger the sphere, the shorter it travels in the vertical

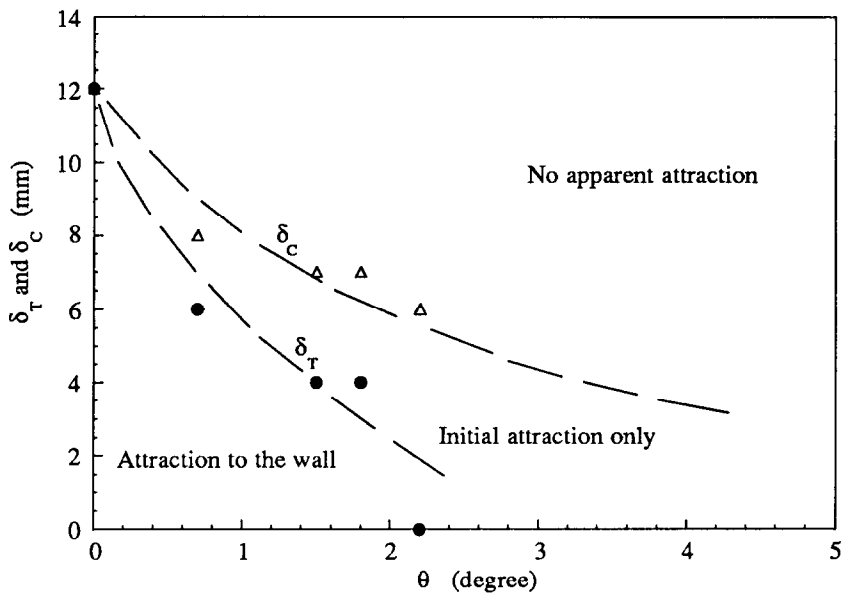
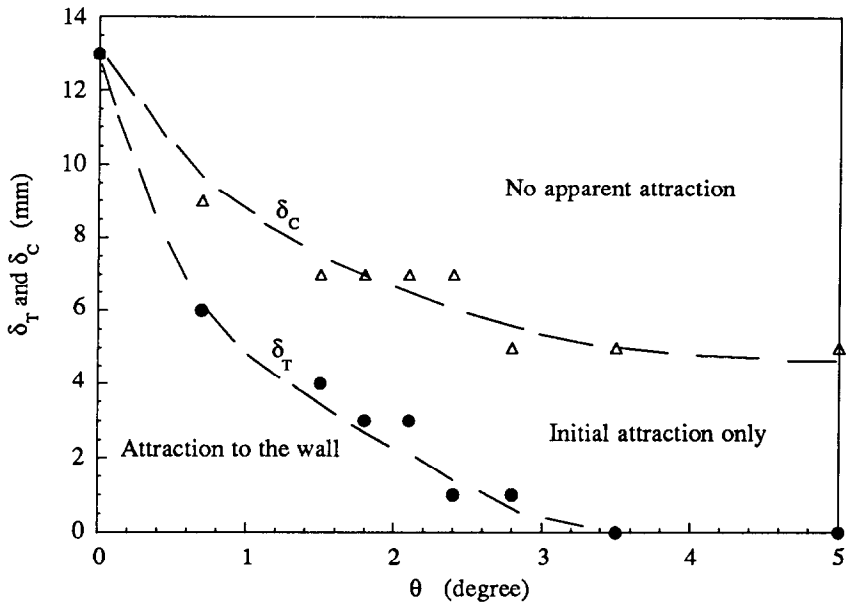


Fig. 26. Critical values of δ between a $\frac{1}{4}$ -in steel sphere and a tilted wall in terms of the critical distances as a function of the tilt angle: (a) 1.25% polyox solution; (b) 1.5% polyox solution.

direction before touching the wall, and the greater the critical distance. Figure 28 plots all data together in the normalized form.

Interactions between a falling sphere and a wall are expressed in terms of the critical touching distances as a function of the tilt angle in Fig. 29. The critical

Table 6
Critical touching and interaction distances in different fluid–solid systems at different tilt angles

Liquid–solid	θ (deg)	δ_T (mm)	δ_C (mm)
Polyox 1.25%–steel	0	13	13
	0.7	6	9
	1.5	4	7
	1.8	3	7
	2.1	3	7
	2.4	1	7
	2.8	1	5
	3.5	0	5
	5	0	5
Polyox 1.5%–steel	0	12	12
	0.7	6	8
	1.5	4	7
	1.8	4	7
	2.2	0	6
S1–steel	0	12	12
	1	2	5
	2	0	5
S1–tungsten	0	10	10
	1	0	5
	2	0	3
S1–teflon	0	3	3
STP–steel		no detectable attraction	
Xanthan–teflon	0	3	3
	1	2	3
	2	2	3
Carbopol–teflon		no attraction	

Table 7
Measured values of the fall velocity and related quantities in the 1.5% aqueous polyox

Spheres	U (cm s ⁻¹)	$\dot{\gamma}$ (s ⁻¹)	Re_0	W_0
$\frac{1}{8}$ -in tungsten	3.44	10.8	0.010	2.17
$\frac{1}{4}$ -in steel	4.13	6.5	0.025	1.30
$\frac{7}{16}$ -in ceramic	5.58	5.02	0.058	1.01
$\frac{5}{8}$ -in aluminum	5.08	3.2	0.076	0.641
$\frac{1}{4}$ -in teflon	0.17	0.27	0.001	0.054
$\frac{1}{4}$ -in aluminum	0.39	0.61	0.002	0.123
$\frac{1}{4}$ -in tungsten	14.6	23	0.087	4.61

touching distance exists only when the tilt angle of the wall is less than about 2°. The critical angles for most spheres tested were between 1.5° and 2° except for the $\frac{1}{4}$ -in. Tungsten sphere for which the critical angle was 1°. Most of the spheres tested have similar critical interaction distances in this case, but the critical distances of the $\frac{1}{4}$ -in. tungsten sphere from a tilted wall are much smaller than the others. The

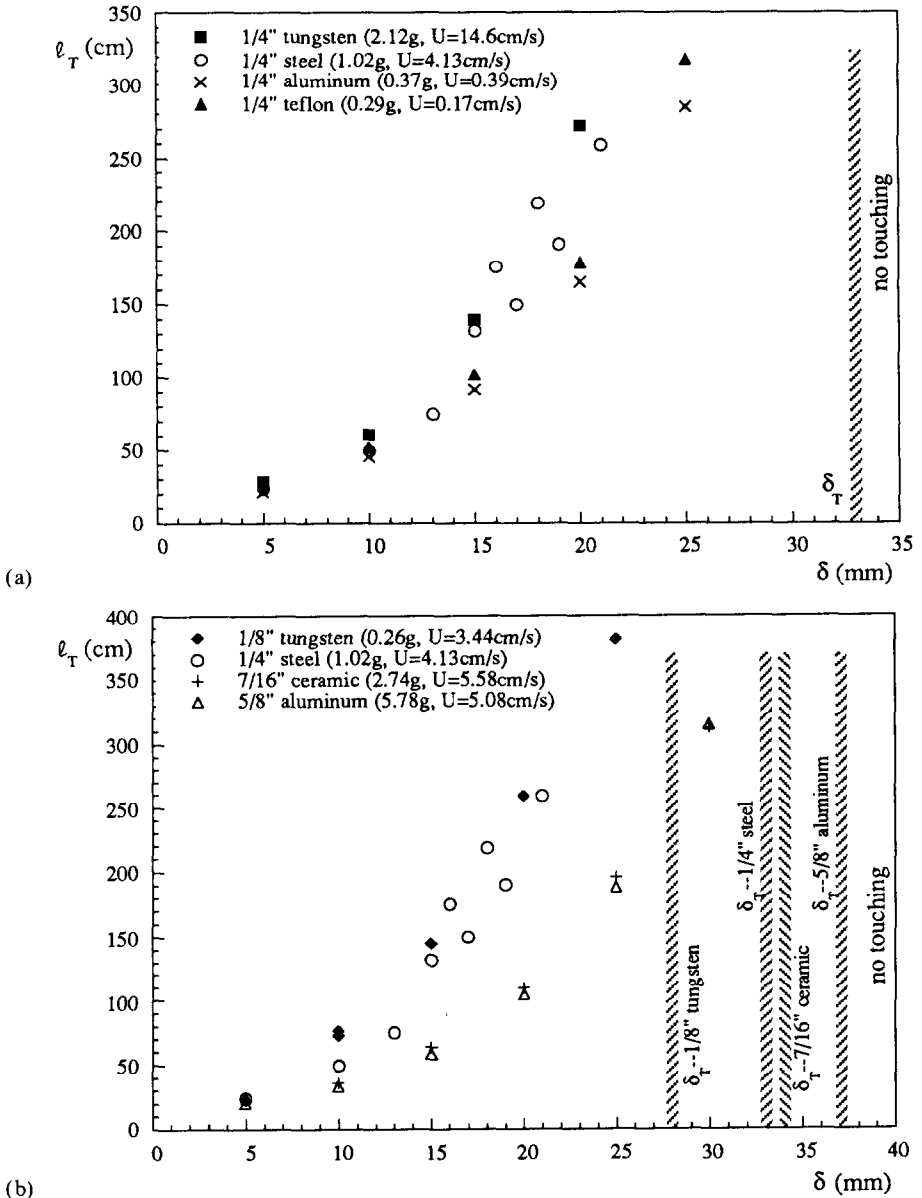


Fig. 27. Interactions between falling spheres and a vertical wall in terms of the vertical distance l_T traveled by the sphere before touching the wall as a function of the initial distance δ between the sphere and the wall in the 1.5% aqueous polyox solution: (a) effect of particle weight; (b) effect of particle size.

experimental results are also summarized in Table 8. The effects of particle size on sphere–wall attraction can also be seen in the case when the wall is tilted through an angle of 1° . Bigger spheres migrate to the wall more rapidly.

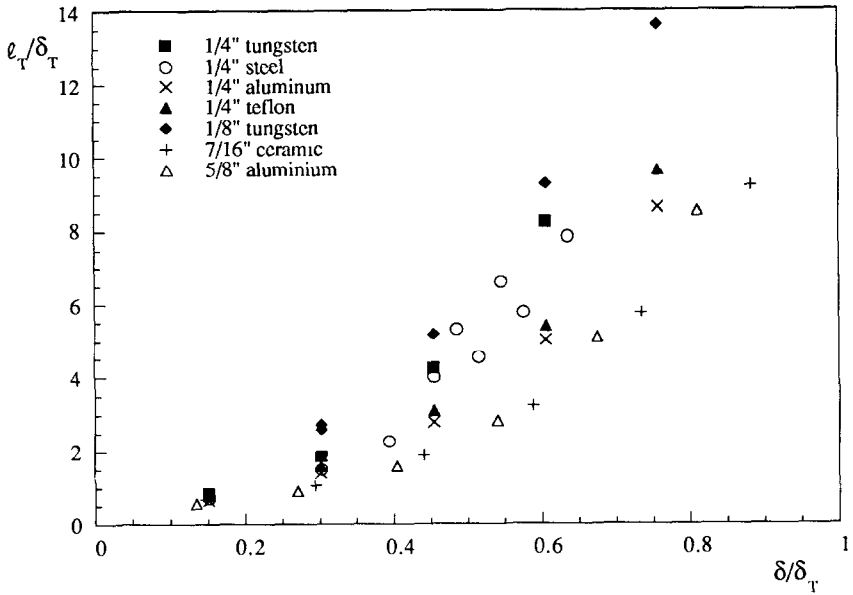


Fig. 28. Normalized form of Fig. 27.

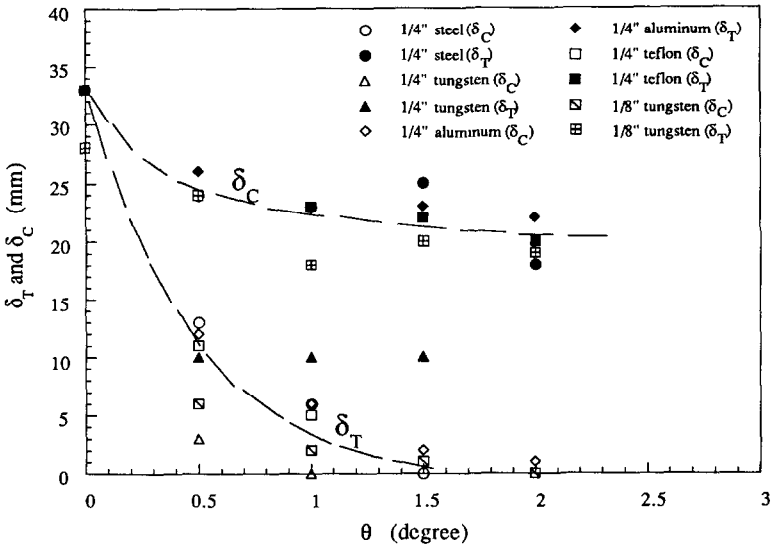


Fig. 29. Critical distances vs. tilt angle of the wall in a 1.5% aqueous polyox. The results given here are similar to those given in Fig. 26.

Table 8
Summary of experimental results in the 1.5% aqueous polyox

Sphere	θ (deg)	δ_T (mm)	δ_C (mm)	δ (mm)	l_T (cm)
$\frac{1}{4}$ -in steel	0	33	33	5	23.9
				5	23.6
				10	49.5
				13	74.9
				15	132
				16	175
				17	150
				18	218
				19	191
				21	259
$\frac{1}{4}$ -in tungsten	0	33	33	5	27.9
				10	61
				15	140
				20	272
$\frac{1}{4}$ -in aluminum	0	33	33	5	21.1
				10	45.7
				15	91.4
				20	165
				25	284
$\frac{1}{4}$ -in teflon	0	33	33	5	25.4
				10	52.1
				15	102
				20	178
				25	318
$\frac{1}{8}$ -in tungsten	0	28	28	5	22.9
				10	76.2
				10	72.4
				15	145
				20	259
				25	381
$\frac{7}{16}$ -in ceramic	0	34	34	5	22.9
				10	35.6
				15	63.5
				20	109
				25	196
				30	312
$\frac{5}{8}$ -in aluminum	0	37	37	5	20.3
				10	33
				15	58.4
				20	104
				25	188
				30	315
$\frac{1}{4}$ -in steel	0.5	13	24		
$\frac{1}{4}$ -in tungsten	0.5	3	10		
$\frac{1}{4}$ -in aluminum	0.5	12	26		
$\frac{1}{4}$ -in teflon	0.5	11	24		
$\frac{1}{8}$ -in tungsten	0.5	6	24		
$\frac{1}{4}$ -in steel	1	6	23	5	71.1

Table 8. (continued)

Sphere	θ (deg)	δ_T (mm)	δ_C (mm)	δ (mm)	l_T (cm)
$\frac{1}{4}$ -in tungsten	1	0	10		
$\frac{1}{4}$ -in aluminum	1	6	23	5	137
$\frac{1}{4}$ -in teflon	1	5	23		
$\frac{1}{8}$ -in tungsten	1	2	18		
$\frac{7}{16}$ -in ceramic	1	11	22	5	35.6
$\frac{3}{8}$ -in aluminum	1	13	22	5	22.9
$\frac{1}{4}$ -in steel	1.5	0	25		
$\frac{1}{4}$ -in tungsten	1.5	0	10		
$\frac{1}{4}$ -in aluminum	1.5	2	23		
$\frac{1}{4}$ -in teflon	1.5	1	22		
$\frac{1}{8}$ -in tungsten	1.5	1	20		
$\frac{1}{4}$ -in steel	2	0	18		
$\frac{1}{4}$ -in aluminum	2	1	22		
$\frac{1}{4}$ -in teflon	2	0	20		
$\frac{1}{8}$ -in tungsten	2	0	19		

7. Discussions and conclusions

We dropped two spheres side-by-side in a sedimentation channel filled with different liquids. In viscoelastic liquids, the spheres will attract when the initial separation distance is small; the line between centers will turn as they attract, until the spheres touch and chain with the line of centers vertical. Close side-by-side settling at slow speeds is unstable in viscoelastic fluids and the dynamics creates stable vertical chains. If the initial side-by-side distance between spheres is large enough, the spheres do not appear to interact, whether or not they are dropped in Newtonian or viscoelastic liquids.

In Newtonian liquids, two spheres launched side-by-side, which are initially separated by a small gap or no gap, will separate. Side-by-side sedimentation is relatively stable or only weakly unstable and spheres will never chain in Newtonian liquids.

Two heavy spheres falling faster than the shear wave speed in a viscoelastic fluid will disperse as in a Newtonian fluid. The phenomenon is the same one that causes long bodies that fall straight down at slow speed to turn 90° into broadside-cross-the-stream fall at supercritical speeds when inertia dominates viscoelasticity.

In the case of attracting spheres, there are two critical values of the initial distances between spheres. For small values of initial distance below the first critical one, the two spheres will come together in a chain with line of centers vertical. If the initial distance between spheres is larger than the first critical value, the spheres would not come together, and if smaller than the second critical value they will move toward one another, but eventually separate.

Spheres that are initially close to a vertical wall or to a wall tilted slightly in such a way that gravity pulls the sphere away from the wall, will attract falling spheres

in a viscoelastic liquid and will repel falling spheres in Newtonian and inelastic liquids. There is a critical separation distance for attraction to a vertical and two critical separation distances, the same ones as for two falling spheres, for the tilted wall. If the angle of tilt is too great (say, greater than 5°) the sphere will always fall away from the wall.

Attraction between spheres and between a sphere and a wall does not depend strongly on the weight or fall velocity of the sphere, but there appears to be a noticeable effect of size, with stronger attractions when the sphere is larger in the sphere-wall experiments. The effects of changing weight is roughly to change the lateral velocity in proportion to the fall velocity.

Our experiments show that different mechanisms promote aggregation in viscoelastic liquids; more than one property is involved. A possible generalization of our observations is that large values of the elastic stress ratio N_1/τ are sufficient but not necessary for strong aggregation. All of the active viscoelastic liquids (polyox solutions and S1), except 0.3% aqueous Xanthan, have large values of N_1/τ and all the liquids except Xanthan, including STP and Carbopol, are nicely ordered with respect to aggregation behavior by the zero shear coefficient of the elastic stress ratio. The Xanthan solution has no measurable normal stresses and the zero shear coefficient of elastic stress ratio, and the ratio itself, are too small to measure, but it has strong properties of aggregation. Xanthan shear-thins strongly and has a large storage modulus. This leads us to believe that shear-thinning plus memory, which creates corridors of reduced viscosity, is also sufficient but not necessary for strong aggregation. In either case the elasticity of the fluid is important. Aggregation seems not to occur in Newtonian fluids or in inelastic fluids with short memory, as in our Carbopol solution or in Boger type fluids with small values of N_1/τ .

Acknowledgments

This work was supported by the NSF, fluid, particulate and hydraulic systems, by the US Army, Mathematics and the Army High Performance Computing Research Center (AHPARC), and the DOE, Department of Basic Energy Sciences. We wish to thank Mr. Dave Hultman who made the “clothespin dropper”, Ms. A.J. Lin who helped in the experimental measurements with the use of an image processing software, Mr. T. Blomstrom, Mr. M. Arney and Ms. S. Braasch, who measured the rod climbing constants, surface tensions, shear wave speeds and viscosities.

References

- [1] Y.J. Liu and D.D. Joseph, Sedimentation of particles in polymer solutions, *J. Fluid Mech.*, 255 (1993) 565–595.
- [2] D.D. Joseph and Y.J. Liu, Orientation of long bodies falling in a viscoelastic liquid, *J. Rheol.*, 37 (1993) 1–22.
- [3] D.G. Christopherson and D. Dowson, An example of minimum energy dissipation in viscous flow, *Proc. R. Soc. London Ser. A*, 251 (1959) 550–564.

- [4] R.I. Tanner, End effects in falling-ball viscometer, *J. Fluid Mech.*, 17 (1963) 161–170.
- [5] B. Caswell, The stability of particle motion near a wall in Newtonian and non-Newtonian fluids, *Chem. Eng. Sci.*, 27 (1972) 373–389.
- [6] L.G. Leal, The slow motion of slender rod-like particles in a second-order fluid, *J. Fluid Mech.*, 69 (1975) 305–337.
- [7] L.G. Leal, Particle motion in a viscous fluid, *Annu. Rev. Fluid Mech.*, 12 (1980) 435–476.
- [8] A.J. Goldman, R.G. Cox and H. Brenner, Slow viscous motion of a sphere parallel to a plane wall. I. Motion through a quiescent fluid, *Chem. Eng. Sci.*, 22 (1967) 637–651.
- [9] P.A. Bungay and H. Brenner, The motion of a closely-fitting sphere in a fluid-filled tube, *Int. J. Multiphase Flow*, 1 (1973) 25–26.
- [10] J.A.C. Humphrey and H. Murata, On the motion of solid spheres falling through viscous fluids in vertical and inclined tubes, ASME 1991 Winter Annual Meeting, Paper No. WAM-91-9.
- [11] D.D. Joseph, J. Nelson, H. Hu and Y.J. Liu, Competition between inertial pressures and normal stresses in the flow induced anisotropy of solid particles, in P. Moldenaers and R. Keunings (Eds.), *Theoretical and Applied Rheology*, Elsevier, Amsterdam, 1992, pp. 60–65.
- [12] Y.J. Liu, J. Nelson, J. Feng and D.D. Joseph, Anomalous rolling of spheres down an inclined plane, *J. Non-Newtonian Fluid Mech.*, 50 (1993) 305–329.
- [13] D. Sigli and M. Coutanceau, Experimental and theoretical investigations of the motion of a sphere in an elastic-viscous fluid with wall effect, in C. Klason and J. Kubat (Eds.), *Proc. 7th International Congress on Rheology*, Swedish Society of Rheology, Goeteborg, 1974, pp. 372–373.
- [14] D. Segli and M. Coutanceau, Effect of finite boundaries on the slow laminar isothermal flow of a viscoelastic fluid around a spherical obstacle, *J. Non-Newtonian Fluid Mech.*, 2 (1977) 1–21.
- [15] M.J. Riddle, C. Narvaez and R.B. Bird, Interactions between two spheres falling along their line of centers in a viscoelastic fluid, *J. Non-Newtonian Fluid Mech.*, 2 (1977) 23–25.
- [16] R.B. Bird, R.C. Armstrong and O. Hassager, *Dynamics of Polymeric Liquids*, John Wiley & Sons, New York, 1987.
- [17] J. Michele, R. Pätzold and R. Donis, Alignment and aggregation effects in suspensions of spheres in non-Newtonian media, *Rheol. Acta*, 16 (1977) 317–321.
- [18] P. Brunn, The slow motion of a rigid particle in a second-order fluid, *J. Fluid Mech.*, 82 (1977) 529–550.
- [19] H. Giesekus, Die Bewegung von Teilchen in strömungen nicht-Newtonscher Flüssigkeiten, *ZAMM*, 58 (1978) T26–37.
- [20] B. Van der Brule and G. Gheissary, Videotape of experiments, unpublished work 1993.
- [21] Y.I. Cho and J.P. Hartnett, The falling ball viscometer—A new instrument for viscoelastic fluids, *J. Heat Mass Transfer*, 6 (1979) 335–342.
- [22] Y.I. Cho, J.P. Hartnett and W.Y. Lee, Non-Newtonian viscosity measurements in the intermediate shear rate range with the falling ball viscometer, *J. Non-Newtonian Fluid Mech.*, 15 (1984) 61–74.
- [23] T.Y. Liao, H.H. Hu and D.D. Joseph, White–Metzner models for climbing in A1, *J. Non-Newtonian Fluid Mech.*, 51 (1994) 111–124.
- [24] G.S. Beavers and D.D. Joseph, The rotating rod viscometer, *J. Fluid Mech.*, 69 (1975) 475–511.
- [25] D.D. Joseph, M.S. Arney, G. Gillberg, H. Hu, D. Hultman, C. Verdier and T.M. Vinagre, A spinning drop tensioextensometer, *J. Rheology*, 36 (1992) 621–662.
- [26] D.D. Joseph, *Fluid Dynamics of Viscoelastic Liquids*, Springer-Verlag, New York, 1990.
- [27] R. Roscoe, The steady elongation of elasto-viscous liquids, *Br. J. Appl. Phys.*, 16 (1965) 1567–1571.
- [28] H.A. Barnes, J.F. Hutton and K. Walters, *An Introduction to Rheology*, Elsevier, Amsterdam, 1989.
- [29] H. Hu, D.D. Joseph and M.J. Crochet, Direct simulation of fluid particle motions, *Theor. Comput. Fluid Dyn.*, 3 (1992) 285–306.
- [30] H. Hu, D.D. Joseph and A.F. Fortes, Experiments and direct simulation of fluid particle motion, *Int. Video J. Eng. Res.*, 2 (1992) 17–24.
- [31] Y. Huang, J. Feng and D.D. Joseph, The turning couples on an elliptic particle settling in a vertical channel, *J. Fluid Mech.*, 271 (1994) 1–16.
- [32] J. Feng, H. Hu and D.D. Joseph, Direct simulation of initial value problems for the motion of solid bodies in a Newtonian fluid. Part 1. Sedimentation, *J. Fluid Mech.*, 261 (1994) 95–134.